İSTANBUL TECHNICAL UNIVERSITY ★ INSTITUTE OF SCIENCE AND TECHNOLOGY

INVESTIGATION OF STRUCTURAL AND ELECTRICAL PROPERTIES OF GAMMA RAYS EXPOSED AL DOPED ZnO FILMS MANUFACTURED VIA SOL-GEL TECHNIQUE

M.Sc. Thesis by
Özge ÖZDEMİR, B.Sc.

Department : Materials and Metallurgical
Engineering

Programme : Materials Engineering

Supervisor: Prof. Dr. Hüseyin ÇİMENOĞLU
Assoc. Prof. Dr. Nilgün BAYDOĞAN

JUNE 2009

İSTANBUL TECHNICAL UNIVERSITY ★ INSTITUTE OF SCIENCE AND TECHNOLOGY

INVESTIGATION OF STRUCTURAL AND ELECTRICAL PROPERTIES OF GAMMA RAYS EXPOSED AL DOPED ZnO FILMS MANUFACTURED VIA SOL-GEL TECHNIQUE

M.Sc. Thesis by
Özge ÖZDEMİR, B.Sc.
(506061430)

Date of submission : 4 May 2009

Date of defence examination : 1 June 2009

<table>
<tr><td>**Supervisor (Chairman) :**</td><td>**Prof. Dr. Hüseyin ÇİMENOĞLU(ITU)**
Assoc. Prof. Dr. Nilgün BAYDOĞAN (ITU)</td></tr>
<tr><td>**Members of the Examining Committee :**</td><td>**Prof. Dr. E. Sabri KAYALI (ITU)**
Prof.Dr.Mehmet KOZ (MU)
Prof. Dr. Sakin ZEYTİN (SAU)</td></tr>
</table>

JUNE 2009

İSTANBUL TEKNİK ÜNİVERSİTESİ ★ FEN BİLİMLERİ ENSTİTÜSÜ

**SOL GEL TEKNİĞİYLE ÜRETİLEN GAMA IŞINLARINA MARUZ
KALMIŞ AL KATKILI ZnO FİLMLERİN YAPISAL VE ELEKTRİK
ÖZELLİKLERİNİN İNCELENMESİ**

**YÜKSEK LİSANS TEZİ
Müh. Özge ÖZDEMİR
(506061430)**

Tezin Enstitüye Verildiği Tarih :	**4 Mayıs 2009**
Tezin Savunulduğu Tarih :	**1 Haziran 2009**

Tez Danışmanı :	**Prof. Dr. Hüseyin ÇİMENOĞLU (İTÜ)**
	Doç. Dr. Nilgün BAYDOĞAN (İTÜ)
Diğer Jüri Üyeleri :	**Prof. Dr. E. Sabri KAYALI (İTÜ)**
	Prof.Dr. Mehmet KOZ (MÜ)
	Prof. Dr. Sakin ZEYTİN (SAÜ)

HAZİRAN 2009

FOREWORD

I wish to thank to my supervisors Prof. Dr. Hüseyin ÇİMENOĞLU and Assoc. Dr. Nilgün BAYDOĞAN, whose suggestions, guidance and encouragement helped me in the carrying out and writing of this thesis. I would also like to express my deep thanks to Cemil IŞIKSAÇAN for his continuous support and invaluable friendship.
I would also like to thank to Asst. Prof. Dr. Murat BAYDOĞAN for his guidance and elaborate critics on my experimental work. I am also indebted to Research Asst. Özgür Çelik, Research Asst. Mert GÜNYÜZ, Asst. Onur Meydanoğlu and my colleagues; Meliha TEKİN, Hale TUĞRAL and İsa Metin ÖZKARA for their supportive attitude and courteous help.

I thank to TUBITAK (The Scientific and Technological Research council of Turkey) for the scholarship, with which they supported me financially during my studies.
And last but not least, thanks to my family, who backed me up under any circumstances for all my life.

May 2009   Özge ÖZDEMİR

                                                             Materials Engineer

TABLE OF CONTENTS

ABBREVIATIONS

ZnO   **:** Zinc Oxide
AZO   **:** Al-doped Zinc Oxide
ITO   **:** Indium Tin Oxide
TCO   **:** Transparent Conducting Oxide
TC   **:** Transparent Conductor
FET   **:** Field Effect Transistor
RT   **:** Room Temperature
SEM   **:** Scanning Electron Microscope
TEM   **:** Transmission Electron Microscopy
FPD   **:** Flat Panel Display
UV   **:** Ultraviolet
PL   : Photoluminescence
QHE   **:** Quantum Hall Effect
RBE   **:** Relative Biological Effectiveness
LET   **:** Linear Energy Transfer
DEA   **:** Diethanolamin

LIST OF TABLES

LIST OF FIGURES

INVESTIGATION OF STRUCTURAL AND ELECTRONIC PROPERTIES OF GAMMA RAYS EXPOSED AL DOPED ZnO FILMS MANUFACTURED VIA SOL-GEL TECHNIQUE

SUMMARY

Zinc oxide is extensively used as varistor, UV light filters, gas sensors and as conductive electrodes in solar cells. For this purpose, extensive research is being carried out to increase the conductivity of zinc oxide with donor doping such as Al^{+3}, In^{+3}, Ga^{+3}.

Therefore, in this study; the effects of Al additions on the electrical and structural properties of ZnO films were investigated with undoped zinc oxide film properties.

Primarily, undoped transparent zinc oxide films were deposited on commercial microscope cover glass via sol-gel dip coating methode. Changes in optical properties were investigated according to effects of sol concentration and annealing temperature difference, by using a spectrophotometer.

Then, Al was doped into the ZnO emulsion in different weigth percentages. By using the same coating technique; new AZO films were applied on Corning 7059 glasses. Optical and electrical properties were evaluated, after at least annealing in five different temperatures, by using spectrophotometer and four point probe, respectively.

Finally, samples were subjected to gamma irradiation. Differences in both structural and electrical properties were concluded.

SOL-GEL TEKNİĞİYLE ÜRETİLEN GAMA IŞINLARINA MARUZ KALMIŞ AL KATKILI ZnO FİLMLERİN YAPISAL VE ELEKTRONİK ÖZELLİKLERİNİN İNCELENMESİ

ÖZET

Çinko oksit yaygın olarak yarı iletken özelliği nedeniyle varistör, UV ışık filtreleri, gaz sensörleri, ve güneş pillerinde elektrot olarak kullanılmaktadır. Günümüzde çinko oksite Al^{+3}, In^{+3}, Ga^{+3} gibi donor katkıları ile iletkenliğinin arttırılmasına çalışılmaktadır.

Bu nedenle, bu çalışmada, katkısız çinko oksit film özelliklerinin yanı sıra, Al eklemenin çinko oksit filmin elektriksel ve optik özelliklerine etkisi incelenmiştir.

Öncelikle, katkısız, şeffaf çinko oksit filmler, ticari mikroskop lameli üzerine sol-gel daldırma yöntemi ile biriktirilmiştir. Optik özelliklerdeki değişimler, sol konsantrasyonu ve farklı tavlama sıcaklıkları göz önüne alınarak, spektrofotometre ile ölçülmüştür.

Daha sonra, ZnO emülsiyonuna farklı ağırlık yüzdelerinde Al eklenmiştir. Aynı kaplama tekniği kullanılarak, yeni oluşturulan AZO filmler Corning 7059 camları üzerine uygulanmıştır. Her numuneye en az beş farklı tavlama sıcaklığı uygulanmış ve nihai ürünün optik ve elektriksel özellikleri sırasıyla spektrofotometre ve dört ayaklı prob ile ölçülmüştür.

Son olarak numuneler gama ışınlarına maruz bırakılmış ve meydana gelen yapısal ve elektriksel özellikler gözlenmiştir.

1. INTRODUCTION

We are seeing high energy prices these days, and it is also being said that the days of low fuel costs are over. It is quite difficult to sustain the present day civilization when the cheap fuel is running out [1].

The combustion of fossil fuel causes global warming. We are witnessing the melting of the polar ice caps at rapid rates. The same is true for many glaciers which feed water to rivers. Major population centers of the world are located on the banks of these rivers [1].

If we continue to burn fossil fuels in the present manner, then it will bring about catastrophic events throughout the world [1].

Solar energy provides us with an alternative where there is no pollution of the environment and its use decreases the rate of depletion of energy reserves [1].

One uses the solar energy in converting this energy into (a) heat, and (b) electricity. In the first case, it is used for directly heating homes or for water heating where the sun's rays are incident on a panel containing circulating water in tubes. In the second case, it is used for generating electricity using photovoltaic panels [1].

There have been different approaches to harness solar energy. In one approach attempts have been made to enhance the energy conversion at the solar cell level by material scientists. The conversion efficiencies range between 12% and 15% of the incident energy [1].

Zinc oxide has recently gained much interest because of its potential use in many applications, ranging from antireflection coatings, transparent electrodes in solar cells, thin film gas sensors, varistors, spitronic devices, photodetecters, surface acoustic wave devices and light emitting diodes to nanolasers, attributed to its wide and direct band gap, excellent chemical and thermal stability, and specific electrical and opto-electronic property of being a II-VI semiconductor with a large exciton binding energy [2].

1

Zinc oxide is one of the few metal oxides which can be used as a transparent conducting oxide (TCO). It has some advantages over other possible materials such as In_2O_3 or SnO_2 due to its unique combination of interesting properties: non-toxicity, good electrical, optical and piezoelectric behavior, stability in a hydrogen plasma atmosphere and its low price. ZnO thin films with high transparency, light trapping and low resistivity properties were studied and used in a broad range of application such as gas sensors, transparent electrodes in display and in photovoltaic devices [3].

Park et al. [4] also suggested that ZnO semiconductor nanowires and nanorods are attractive components for nanometer scale electronic and photonic device applications. Recently, a wide variety of nanodevices including ultraviolet photodetectors, Schottky diodes, and light emitting device arrays have been fabricated utilizing ZnO nanorods (nanowires). In particular, a field effect transistor (FET), one of the most fundamental and important electronic components has been fabricating ZnO.

Özgür et al. [5] indicated that ZnO is not really a new discovered material. Research on ZnO has continued for many decades with interest following a roller-coaster pattern. Interest in this material at the time of this writing is again at at a high point.

In terms of its characterization, reports go back to 1935 or even earlier. For example lattice parameters of ZnO were investigated for many decades. Similarly optical properties and processes in ZnO as well as its refractive index were extensively studied many decades ago. Vibrational properties by techniques such as Raman scattering were also determined early on. Investigations of ZnO properties presume that ZnO samples were available. Growth methods not much different from what is employed lately have been explored, among which are chemical-vapor transport, vapor-phase growth, hydrothermal growth [5].

The ZnO bulk crystals have been grown by a number of methods, as has been reviewed recently, and large-size ZnO substrates are available. High-quality ZnO films can be grown at relatively low temperatures less than 700 $^\circ$ C . The large exciton binding energy of 60 meV paves the way for an intense near-band-edge excitonic emissions at room and higher temperatures, because this value is 2.4 times that of the room-temperature (RT) thermal energy (k_BT=25 meV). There have also been a number of reports on laser emission from ZnO-based structures at RT and

beyond.

It should be noted that besides the above-mentioned properties of ZnO, there are additional properties which make it preferable over other wide-band-gap materials: its high- energy radiation stability and amenability to wet chemical etching [5].

Several experiments confirmed that ZnO is very resistive to high-energy radiation, making it a very suitable candidate for space applications. ZnO is easily etched in all acids and alkalis (Figure 1.1), and this provides an opportunity for all acids and alkalis, and this provides an opportunity for fabrication of small size devices [5].
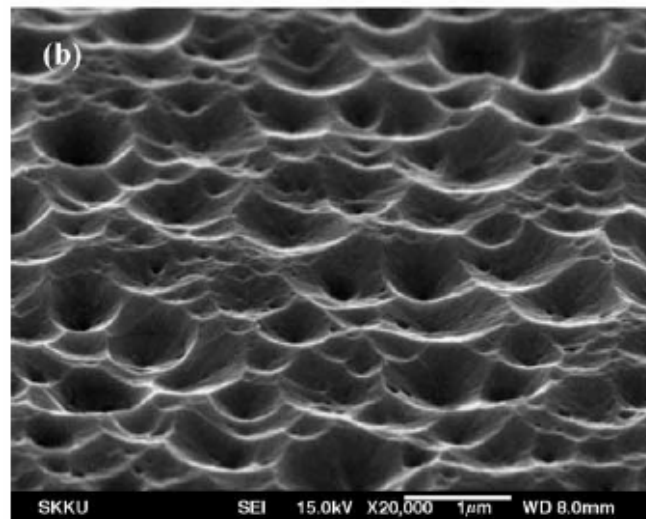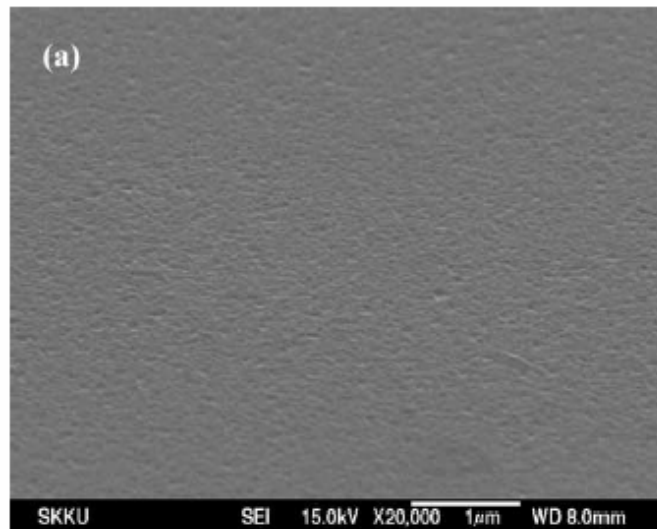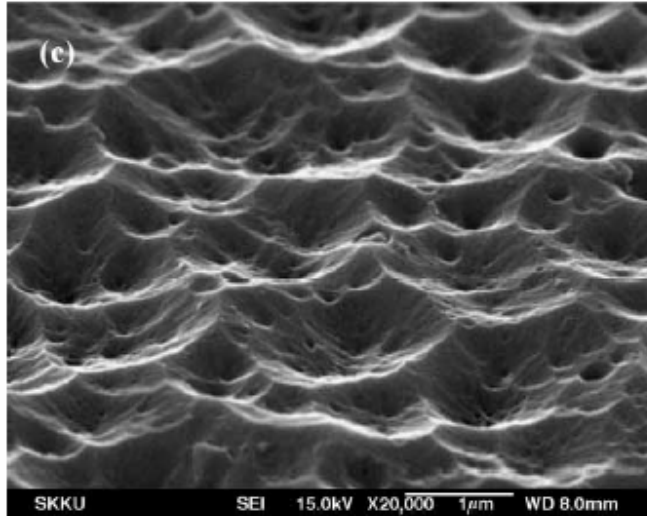
Figure 1.1: SEM image of the Al:ZnO thin films, smooth and etched by %0.5 HCl, (a) without etching, (b) etched for 20 s. and (c) etched for 60 s. [6]

By controlling the doping level electrical properties can be changed from insulator through *n*-type semiconductor to metal while maintaining optical transparency that makes it useful for transparent electrodes in flat panel displays and solar cells. However, one important problem should be overcome before ZnO could potentially make inroads into the world of optoelectronics devices: the growth of *p*-type conductivity ZnO crystals. Despite all the progress that has been made and the reports of *p*-type conductivity in ZnO films using various growth methods and various group-V dopant ele ments N, P, As, and Sb , a reliable and reproducible high quality *p*-type conductivity has not yet been achieved for ZnO. Therefore, it remains to be the most pivotal topic in ZnO research today, and congruently most of the research efforts are directed just to solving this problem. In order to overcome this bottleneck and to control the material's properties, a clear understanding of physical processes in ZnO is necessary in addition to obtaining low *n*-type background. In spite of many decades of investigations, some of the basic properties of ZnO still remain unclear. For example, the nature of the residual *n*-type conductivity in undoped ZnO films, whether being due to impurities of some native defect or defects, is still under some degree of debate. Some authors ascribe the residual background to intrinsic defects (oxygen vacancies, V_0, and interstitial zinc atoms, Zn_i), and others to noncontrollable hydrogen impurities introduced during growth. The well-known green band in ZnO luminescence spectra manifesting itself as a broad peak around 500 – 530 nm ,

4

observed nearly in all samples regardless of growth conditions, is related to singly ionized oxygen vacancies by some and to residual copper impurities by others [5].
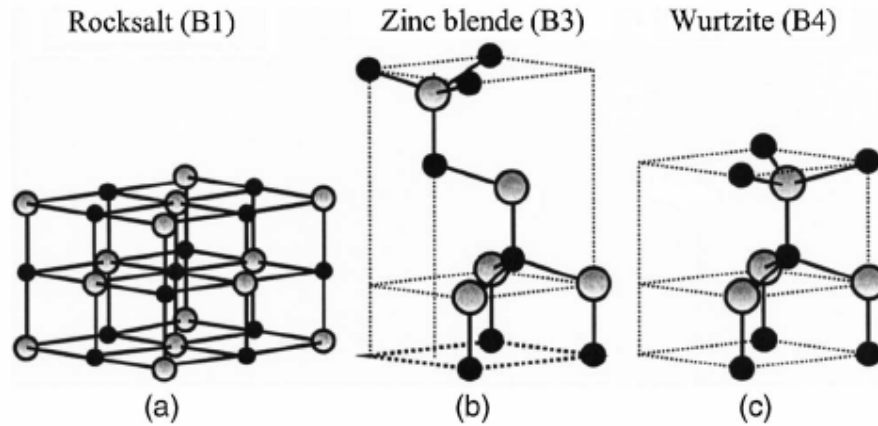
Figure 1.2: Stick and ball presentation of ZnO crystal structures; (a) cubic rocksalt (B1), (b) cubic zinc blende (B3), (c) wurtzite (B4). Shaded grey and black spheres donate Zn and O atoms, respectively   [5]

ZnO is a II-VI compound semiconductor whose ionicity resides at the borderline between covalent and ionic semiconductor. The crystal structures shared by ZnO are wurtzite (B4), zinc blende (B3), and rocksalt (B1) as schematically shown in Figure 1.2 (a),(b) and (c). At ambient conditions, the thermodynamically stable phase is wurtzite. The zinc-blende ZnO structure can be stabilized only by growth on cubic substrates, and the rocksalt NaCl structure may be obtained at relatively high pressures [5].

The band structure of a given semiconductor is pivotal in determining its potential utility. Consequently, an accurate knowledge of the band structure is critical if the semiconductor in question is to be incorporated in the family of materials considered for device applications. Several theoretical approaches of varying degrees of complexity have been employed to calculate the band structure of ZnO for its wurzite, zinc-blende, and rocksalt polytypes. Besides, a number of experimental data have been published regarding the band structure of the electronic states of wurtzite ZnO. X-ray or UV reflection/absorption or emission techniques have conventionally been used to measure the electronic core levels in solids. These methods basically measure the energy difference by inducing transitions between electronic levels for example, transitions from the upper valence-band states to the upper conduction-band states, and from the lower valence-band states or by exciting collective modes for example,

the upper core states to the lower edge of the conduction band and to excitations of plasmons [5].

Using transmission electron microscopy, Tse et al. [7] showed the ZnO structure together with silicone substrate (Figure 1.3). A columnar growth structure was found in ZnO thin films with an amorphous layer several nanometers thick at the interface between the substrate and polycrystalline ZnO films [8, 7].
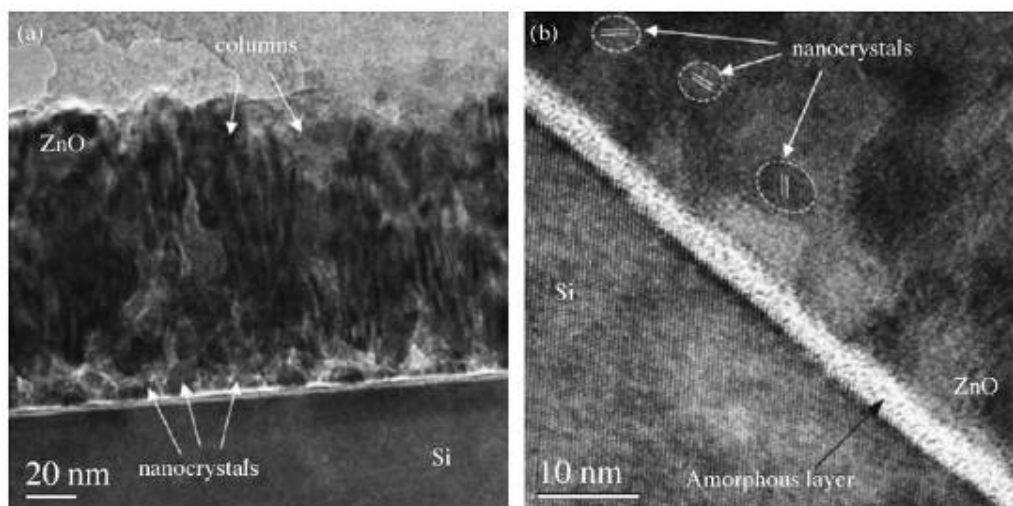
Figure 1.3: TEM micrograph of ZnO thin films deposited at room temperature (a) brigth field image and (b) lattice image at the interface [7].

ZnO:M (M=Al, Ga, In) thin films with high *c*-axis orientated crystalline structure along (002) plane are extensively studied for practical applications including transparent conducting electrode materials for various electronic devices such as solar cells, electroluminescence displays, etc. A high degree of crystal orientation reduces the electrical resistivity due to an increase in carriers mobility by reducing the probability of the scattering of the carriers at the grain boundary [9].

However, the reasons for these low conductivity values as well as the dependence of the electrical properties on the preparation technique have not been elucidated, probably because of the complex structure of zinc oxide and the number of parameters involved even for a single film processing technique [10].

It is well known that chemical doping greatly influences the electronic and optical properties of ZnO. Doped ZnO thin films are of technological importance becouse of their great potential for various applications such as transparent conducting electrodes (doping with III A elements), insulating or dielectric layers (doping with Li), and spintronic devices (doping with Mn) [2].

Among them, Al-doped ZnO compounds are the most conventional transparent conductive oxides (TCOs), which are useful as transparent electrodes (opto-electronic devices) or as thermal insulator films in smart windows (low emissive windows) [11].

Despite these advantages, relatively few reports deal with the sol-gel preparation of AZO transparent conductors. Most of the work has been done on AZO thin films deposited mainly by physical methods. Coatings with satisfactory electrical conductivities have been successfully deposited by sputtering. On the other hand, one order low values are reported for the sol-gel coated films [10].

Al doped ZnO (AZO) films are known as n-type direct band gap semi conductors with optical transparency. Recently, a drastic increase has been observed in the conductivity of AZO films by irradiation of both low energy and high energy ions, and low energy ion irradiation followed by annealing. It has been suggested that the conductivity increase originates from enhancement of both the carrier density due to replacement of Zn site by Al and mobility by ion irradiation. The modifications of the electrical properties are expected to link to those of other prperties such as optical and structural properties [12].

In recent years, many researchers have attempted to provide a more accurate estimation of the Al^{3+} solubility limit in ZnO. In literature, this solubility limit has been studied on powder as well as on thin films [11].

Al-doped ZnO compounds are often characterized in their final shape that is TCO thin films, elaborated from magnetron sputtering or other physical vapour deposition processes or more scarcely by dip/spin coating [11].

Investigation of the composition of these thin films using X-ray diffraction remains difficult because of various artefacts, which hinder the observation of possible other minor phases:

- small amount of matter due to film thickness,

- strong intensity of diffraction peaks caused by epitaxial film growth,

- presence of the substrate peaks when the latter is a crystallized material, etc. [11].

Many methods have been employed to prepare ZnO thin films like spray pyrolysis, molecular beam epitaxy, chemical vapor deposition, RF magnetron sputtering and sol–gel. The latest method has the advantage to give a high surface morphology at lower crystallizing temperature [13].

Sol-gel processing is a versatile method for depositing oxide based coatings on a variety of substrates in an economical manner. Literature reports the use of sol- gel coating to give optical properties like antireflecting, non-linear, luminescent or thermochromic [14, 15].

Another advantage of sol-gel is the possibility small area as well as large area coating of films at a low cost for technological applications [16].

Conventional sol–gel deposition of AZO involves two high-temperature steps for preheating and annealing, respectively. The two steps are required to heat up the sample to 450 °C to 500 °C. The function of preheating is to remove organic impurities while annealing is to enhance crystal growth. However, such temperatures are unacceptably high for substrates with a low glass transition temperature such as plastics. Therefore, the aim of using excimer laser irradiation instead of conventional annealing process is to minimize heating and damage to the substrate (limit the heating to precursor AZO films with minimal heating on the substrates) due to selective laser absorption by the overlaying film. Besides, laser irradiation is also expected to have direct photoinduced influence, which leads to rapid crystallization of the precursor films and atom dissipation from the film. In semiconductor industry, pulsed laser annealing has been applied to improve the structural, optical and electrical characteristics of polycrystalline semiconductor films [17].

The sol-gel method has also been employed to produce ZnO thin films by using different zinc sources (e.g., zinc nitrate, zinc acetate, and zinc ethoxides and propoxides) and other additives (e.g., different amines as catalysts). Such changes have resulted in precursor solutions of different compositions, which in turn lead to ZnO films with different characteristics [18].
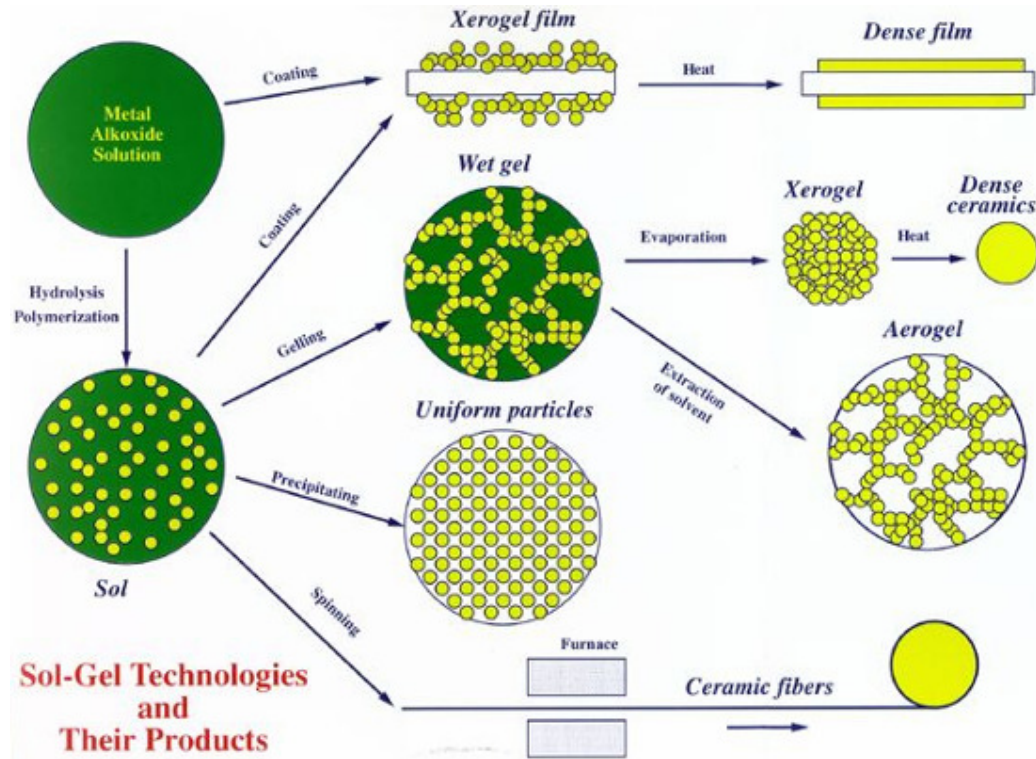
Figure 1.4: Solgel technologies and their products [19].

The sol–gel process is based on hydrolysis and polycondensation reactions (Figure 1.4) and has advantages over other processes due to its simplicity and low equipment cost. In general, metal alkoxides are used as raw materials, but the preparation of the sols can be difficult because of their reactivity. Furthermore, the alkoxides are very expensive and are insoluble in most alcohols. For this reason, the interest in inorganic sol–gel routes has significantly increased in the last years, since the raw materials used have lower cost. However, it is verified that few are the papers bringing some information on the initial steps of ZnO or doped ZnO film formation via inorganic routes [20].

2. SOL-GEL TECHNIQUE

Coatings are widely used in optical, microelectronic, packaging, biomedical and decorative applications. The coating is designed to impart favorable mechanical (i.e. low friction, abrasion resistance), chemical (i.e. barrier for gasses), optical, magnetic, and electrical properties to various substrates [21].

In general, the functional behaviour of these coatings depends on the bulk or surface properties of the coating material. Evidently, the durability and functionality of coatings is critically dependent on the adhesion between the coating and the underlying substrate [21].

As substrates, transparent conductors (TCs) are usually preferred [22].

The TCs used for solar energy and energy efficiency are normally thin films, with thicknesses between 10 nm and 1μm, backed by transparent or non-transparent substrates [22].

As Li et al. suggest [23], ZnO is a potential substitute transparent conducting oxide and ZnO thin films have been prepared by a variety of thin film deposition techniques, such as pulsed laser deposition, RF magnetron sputtering, chemical vapour deposition, spray pyrolysis, electrodeposition, sol-gel process, etc [24].

The sol-gel method is an alternative means to form coatings and has several advantages: changing the chemistry or processing conditions can modify the microstructure of coatings. Additionally, sub-micron thin films of uniform thickness can be made using sol-gel techniques [25].

The sol–gel synthesis of materials based on the hydrolysis and condensation of molecular precursors is used to prepare a wide range of inorganic materials. This procedure gives sols, colloidal particles suspended in a liquid that progress through a gelation process to finally form two interpenetrating networks—the solid phase and the solvent phase. Although the roots of sol–gel chemistry can be traced to the 19th century, only during the past 30 years has the field witnessed remarkable growth in sophistication and applications. Increased interest in sol–gel materials has paralleled the emergence of materials chemistry and the recognition of the vast common ground between the chemistry and materials science communities [26].

It is tempting to consider the 1970s as the era of the rise of the sol–gel materials field, but there were a number of earlier contributions that demonstrated some of the types of materials available with this synthesis approach. The sol–gel synthesis of colloidal particles and the deposition of thin films date back to the 1950s. Thus, sol–gel approaches were used to prepare nanodimensional inorganic materials well before the terms nanoscience and nanotechnology were popularized. Beginning in the late 1970s, researchers active at the interface between chemistry and materials science recognized the possibilities provided by sol–gel methods. Much of this interest evolved from glass science, since the ability to form inorganic glasses without melting, the synthesis of glass compositions that could not be achieved by melting, and the ability to exploit the solution nature to form glasses as fibers, films, or bulk materials (termed monoliths) represented an extraordinary combination of potential opportunities. The renewed interest in sol–gel materials occurred at a time when noncrystalline solids were being widely investigated for uses in optical communications. Multiple contributions to this special issue show the continuing active interest in sol–gel methods for optical applications, but emphasis has evolved from the scientific understanding of optical properties to the design of sol–gel materials as optical components and devices [26].

This special issue highlights several of the most scientifically and technologically active areas in the sol–gel field. The papers are organized roughly into five categories: studies of silica-based sol–gel materials, non-silica-based materials, sol–gel biological materials, porous sol–gel materials, and optical sol–gel materials. One of the underlying themes in several papers is the growing sophistication in synthesizing materials with designed chemistry and morphology. This is particularly evident when authors discuss hybrid materials. These materials are largely based on the use of sol–gel approaches to combine organic and inorganic functionalities. The versatility demonstrated in these materials is exceptional, as the range of materials extends from those with local organic groups attached to an inorganic framework to those materials composed of interpenetrating organic and inorganic networks. For a number of years, sol–gel methods have been used to synthesize an exciting generation of materials at the interface between physical science and biology. The contributions to this special issue show the breadth of this active research area and its emerging applications [26].

Another unique feature of sol–gel materials is control of pore solid architecture. There is extraordinary control not only of the size (mesopores of 2–50 nm) but also the arrangement of pores within the inorganic (or organic/inorganic) framework. The design of materials with specific architectures is enabling researchers to obtain unique properties in such diverse areas as drug delivery and electrochemistry [26].

2.1 Dip Coating Technique

Dip application of a coating involves simply immersing a work piece into a suitable tank containing the coating material, allowing the part to drain after withdrawal and force drying or baking the wet coating to achieve the finish (Figure 2.1). Dip coatings are used in many industries for both primer and one-coat finishes [27].

Thorough cleaning of parts is essential prior to dipping [27].

①dip the base into the solution

②sink the base perpendicular to the solution and wait for the solution surface to be calm.

③pull up the base at the certain speed perpendicular to the solution surface.

The target particles align regularly for the fluxion from capillary force and evaporation.

④the thickness can be controlled by the speed of step 3 or the concentration of the solution.

Figure 2.1: Dip coating principles [28].

2.1.1 Benefits of Dip Coating

Simplicity: Manpower and equipment requirements are minimal. The process is easily automated [27].

Low Cost: Paint utilization should be relatively high (e.g., greater than 90% transfer efficiency) on properly operated systems, since nonused paint (drainage) is mostly recovered and returned to the system [27].

Ease of Control: Minimally skilled operators can maintain solids, viscosity, and other factors for acceptable application properties [27].

Good Coverage: Except for air bubbles or pockets, all contact areas are coated. Close racking of parts is possible [27].

Consistency: Similar parts receive coatings similar in appearance and film thickness (i.e., the process is independent of the operator) [27].

2.1.2 Limitations

Nonuniform Coatings: "Wedges" (thin films on upper surfaces, thicker on lower surfaces) tend to form on vertical surfaces. Flow lines around holes or openings can also occur. "Beads" on bottom edges are inherent defects, although proper viscosity control can minimize this effect [27].

Part Design and Hanging: Improperly racked parts can bucket paint, leading to waste and potential blistering in the puddled areas. Entrapped air pockets can prevent access of paint, with resultant bare areas. It may be necessary to design drain/access holes into some work to allow for immersion application. An attempt should be made to rack a part so that drainage occurs from a single point. Oscillation during immersion can sometimes remove air pockets [27].

Solvent Washing: Entrapped solvent during the curing process can resolubilize an already dried film, resulting in bare areas [27].

Product Change: A change from one formulation to another requires either extensive cleaning or recharging of a single tank or the availability of multiple dip tanks. Thoroughness of clean-out is especially important when switching incompatible materials (e.g., replacing a solvent-borne system with a waterborne system) [27].

Flammability: The potantial of fire is always present when solvent-borne dip primers are used. With water-borne systems this problem is greatly reduced [27].

Foam: Undesirable foam, which usually originates in the paint recirculation system,can produce voids or craters in the final finish. This problem is more prevalent with waterborne paints [27].

Sticking: Small objects, such as fasteners processed in baskets or trays, can fuse together during cure. Processes such as autodeposition or electrodeposition that utilize water rinsing following the coating tank generally do not produce this effect [27].

Viscosity: Control is critical. High viscosity gives thick films and excessive consumption. Low viscosity produces films [27].

2.1.3 Typical Coatings Used

Selection of coating system (i.e., resin type, pigment color) is directly related to the performance intended for the finished parts. Although any formulation with the appropriate viscosity for acceptable transfer efficiency (i.e., greater than) 90% can be usedi properties of appearance, quality, cost, and other factors must be taken into account [27].

There is a trend toward the use of waterborne formulations because these are both fire resistant and ecologically desirable. Defoamers are often required to control foam in waterborne systems; however, silicone-containing materials must be avoided. Waterborne paints are often more aggressive toward equipment than solventborne formulations [27].

2.1.4 Equipment Requirements

If high-volume throughputs are desired, a continuous conveyor for work transfer is usually employed in contrast to a manual or programmed hoist. Circulating pumps are required to maintain uniform viscosity and constant paint composition. The "bead" that characteristically forms on the lowermost edge of a draining part is sometimes removed by ultrasound, by electrostatic detearing, or by air jets; the latter is generally the least expensive technique [27].

A controlled withdrawal rate is useful in controlling coating thickness. This is more readily varied with a hoist system [27].

2.1.5 Maintenance

Floating residues must be removed from the paint tank to prevent clinging of the material on withdrawn work pieces. This is usually accomplished bu periodic skimming [27].

Overhead conveyor systems require lubrication for maximum life. However, any lubricants should be pretested as potential contaminants in the paint because some materials can cause cratering and other defects in the final product [27].

Racks must be periodically stripped of dried paint. Either stripping (molten salt bath or high-temperature oven), cryogenic stripping (exposure to liquid nitrogen, followed by physical removal of the embrittled paint), or media blasting (sand, steel shot) can be used [27].

Cleaning of the drain-off area must occur on a regular basis. Care must be taken to avoid getting dried paint into the circulation system, with resultanat damage to filters, pumps, and nozzles [27].

2.1.6 Dip Coating Theories

Numerous experimental and theoretical studies of the dip-coating process are to be found in the literature. Meng and coworker used a model to quantitatively describe wet membrane formation on a porous substrate by capillary filtration during the dip-coating process. The model is derived on the basis of the slip-casting process, and the effect of the withdrawal speed of the substrate on the thickness of the top layers has not been considered. Krozel et al. investigated the fluid mechanical aspects of halted substrate motion using gravimetric means, based on the following two basic theoretical models: (1) Jeffrey's solution for transient coating and drainage, where capillary forces were considered to be negligible; (2) the Landau–Levich solution for steady state coating, which was modified by White and Tallmadge. In the latter model the effect of dipping time on the thickness of the top layers was also not considered. Other researchers have used these models for ceramic membrane formation by the dip-coating processes [29].

Dipping Time Theory

Dipping time theory has been recently developed for ceramic membrane formation by the dip-coating process. In this model, the growth of film thickness (h_{ave}) is interpreted as a function of substrate permeability (K_s) and of the permeability of the film (K_m) previously deposited on the substrate (Babaluo, 2004):

$$h_{ave} = 2\left[\frac{\varepsilon_s \sigma}{\eta \alpha R[(1/K_m) + (\alpha/\varepsilon_s)(1/K_s)]}t\right]^{1/2}$$

(2.1)

where ε_s is the substrate porosity, t is the dipping time (s), η is the viscosity of suspension (N m^{-2} s), σ is the surface tension of the liquid (solvent) in the pores of the support (N m^{-1}), R is the radius of support pores (m), and α is defined as (Babaluo, 2004):

$$\alpha = \frac{\phi_m}{\phi_0} - 1$$

(2.2)

where φ_0 and φ_m are the volume fractions of the particles in the suspension and in the wet membrane, respectively.

Usually, the permeability of the substrate (K_s) is much bigger than that of the membrane (K_m), therefore, Equation (2.1) is simplified as follows:

$$h_{ave} = 2\left(\frac{\varepsilon_s \sigma K_m}{\eta \alpha R}t\right)^{1/2}$$

(2.3)

Considering the membrane shrinkage during the drying and sintering processes, the thickness of the sintered membrane ($h_{ave,s}$) can be expressed as:

$$h_{ave,s} = \beta h_{ave} = 2\beta \left(\frac{\varepsilon_s \sigma K_m}{\eta \alpha R} t \right)^{1/2}$$

(2.4)

where β is defined as:

$$\beta = \frac{\phi_m}{1 - \varepsilon_m}$$

(2.5)

ε_m is the porosity of the sintered membrane.

The film permeability is determined by the following equation:

$$K_m = \frac{\varepsilon_m^3}{K_0 K_T S_v^2 (1 - \varepsilon_m)^2}$$

(2.6)

where K_0 is a particle shape factor and K_τ accounts for the tortuosity of the porous medium. The product of K_0 and K_τ was generally put at about 5 for particle packings. S_v is the surface area of the particles per unit volume of the solid (m^{-1}) [29].

19

Withdrawal Speed Theory

For Newtonian liquids, the principle considered in the prediction of the Landau–Levich model is the limiting film thickness (h_∞):

$$h_\infty = 0.944\frac{(\eta U)^{2/3}}{\sigma^{1/6}(\rho g)^{1/2}}$$

(2.7)

where ρ is the density (g m^{-3}), g is the acceleration due to gravity (m s^{-2}) and U is the withdrawal speed of the substrate (m s^{-1}). It is customary to introduce a scaled film thickness (T) and a capillary number (N_{ca}) as follows:

$$T = h\left(\frac{\rho g}{\eta U}\right)^{1/2}$$

(2.8)

$$N_{ca} = \frac{\eta U}{\sigma}$$

(2.9)

So that the Landau–Levich expression may be written as (at $h=h_\infty$):

$$T_\infty = 0.994 N_{ca}^{1/6}$$
(2.10)

This theory is valid for $N_{ca} \square\square 1$. The constant thickness region (II) in Figure 2.2, typically constitutes the majority of the film on the substrate, and pertains to Landau–Levich theory. White and Tallmodge patched regions (I) and (II) together to obtain the average film thickness for constant withdrawal speed:

$$T_{ave} = 0.994 N_{ca}^{1/6}\left[1 - 0.297\left(\frac{\eta U}{\sigma}\right)^{1/3}\right]$$

(2.11)

or

$$h_{ave} = 0.994 \frac{(\eta U)^{2/3}}{\sigma^{1/6}(\rho g)^{1/2}} \left[1 - 0.297 \left(\frac{\eta U}{\sigma} \right)^{1/3} \right]$$

(2.12)
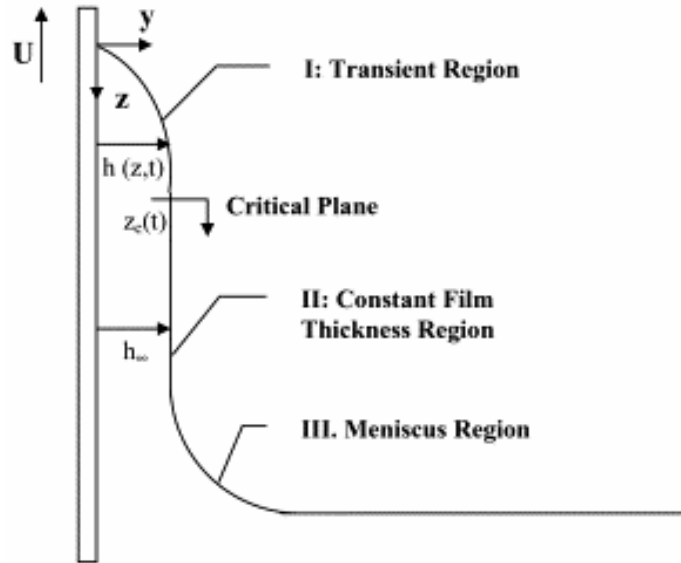
Figure 2.2: An instantaneous view of a dip-coating process. Three major regions are labelled. The critical plane separates regions (I) and (II) from Babaluo, 2004 [29].

It is believed that a modified model could be used to induce better quality in products, better process control, and consistency [29].

3. ELECTRICAL PROPERTIES OF TRANSPARENT MATERIALS

During the last two decades; the size of the electronic devices and systems has been decreased continously and recently nanometer scale range was attained. Unusual properties and performances have been obtained with nanostructured materials. Ultrathin metal films are an important part in electric devices and systems and their electrical conductivity has been paid some attention [30].

The electrical properties of materials depend significantly on processes that influence the conductivity of the sample proper. Such processes, in particular, carrier blocking at the electrodes, the formation and relaxation of space charges, and intergranular barriers, occur at the electro-sample interface. The contribution of these processes to the total conductivity of the sample can be assessed by measuring its impedance in a wide frequency range [31].

Transparent conductive oxides (TCO) films have been widely used as optoelectronic devices such as touch panels, flat panel displays (FPD), and thin film solar cells. For display applications with high quality the TCO films should have high optical transmittance in the visible region and high electrical conductivity [29].

Impurity-doped zinc oxides (ZnOs) are widely accepted as substitudes for TCO because of the advantages of low cost, resourse availability (about a factor of 1,000 more than indium), nontoxicity and high thermal/chemical stability [29].

Undoped ZnO usually presents a high resistivity due to a lower carrier concentration. Enhancement of the elctrical properties of TCOs, specifically conductivity, can be achieved by increasing either the carrier concentration or the carrier mobility. Aluminium (Al), indium (In) and galium (Ga) had been reported as effective dopants for zinc oxide-based TCO films [29].

Since the import of III-group element, the Al doping can dramatically increase the free carriers concentration and simultaneously keep the transparency in the visible range (Figure 3.1). Both these are necessary for the transparent conduction. Many methods have been employed to obtain the AZO thin films and the conduction mechanism was extensively discussed based on the energy band structure [32].

Dopant	Transmittance in visible range	Lowest resistivity	Methods
Al	~90%	~10^{-4} Ωcm	Pulsed laser deposition (PLD)
			Radio-frequency (RF) magnetron sputtering
			Solution processed
Ga	~85%	~10^{-3} Ωcm	PLD
			Solution processed
In	~80%	~20 Ωcm	Solution processed
N	~80%	~10^{-2} Ωcm	Plasma-assisted molecular beam epitaxy
			RF magnetron sputtering
			Solution processed

Figure 3.1: Optical and electrical properties of III-group elements [33].

Among the ZnO films doped by these elements Al-doped zinc oxide (AZO) films show the lowest electrical resistivity. AZO films are also wide band gap semiconductors (E_g = 3.4-3.7 eV), which have high optical transmittance in the visible wavelength region. However, a further decrease in the resistivity is required for future display technology applications [29].

The electronic energy levels of native imperfections in ZnO are illustrated in Figure 3.2.
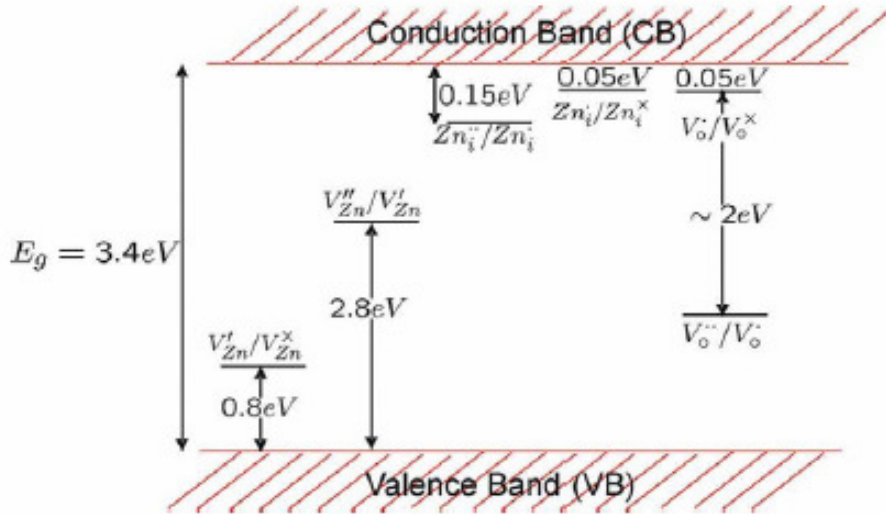
Figure 3.2: Electronic energy levels of imperfections in ZnO [33].

3.1 Plasma Frequency in Conductive Structures

The application fields of transparent conductive oxides (TCOs) are vast and increasing in the last years. Besides the flat panel industry, photovoltaics has emerged as a major industrial branch in need for high quality transparent conducting oxides. The development of large area deposition processes for these layers has experienced a boost with industrialization of thin-film concepts, e.g. solar cells based on thin-film silicon or compound semiconductors like CuInS and related materials [34].

A simple requirement posed on the TCO film in this context is a high optical transmission for photon energies above the bandgap of the absorber material used. As an example the bandgaps of polycrystalline and hydrogenated microcrystalline silicon are around 1.1 eV. This means that the spectral range in which the TCO layer should exhibit high transmission will reach up to 1100 nm. This requirement is not met by many TCO films as, depending on doping level, they can have a considerable absorption in this range [34].

The decreased transmission towards higher wavelength s is caused by free carrier absorption. This means that the optical behavior of TCO films is strongly linked to the electrical transport properties. This is described by the Drude theory [34].

The results of the modeling procedure can be used to investigate the link age of optical and electrical performance of the films used during experiments. As will be seen the effective mass $m*$ of the electrons in the conduction band is a key parameter to understand the link of optical and electrical behavior of TCO materials. Only the assumption of a non-parabolic conduction band in ZnO leads to an accurate determination of carrier concentration from optical spectroscopy [34].

Finally, the information gained on the conduction band form is used to also determine the carrier mobility from the optical spectra [34].

Drude Theory and Extentions

The trade off between optical transmission and electrical conductivity of TCO layers demands a profound knowledge of the connection of the two material properties. The basic theory of the optical behavior of free carriers in solids has been formulated by Drude and is described in various textbooks and articles. In his theory the susceptibility accounting for the free carriers can be expressed as;

$$\chi^{FE} = -\frac{\omega_p^2}{\omega^2 + i\omega\omega_\tau}$$

(3.1)

Where ω_p donates the plasma frequency and ω_τ is a damping term. ω_p is a function of the carrier density N_e, while the damping depends on the mobility μ;

$$\omega_p^2 = \frac{e^2 N_e}{\varepsilon_0 m_{opt}^*}$$

(3.2)

$$\omega_\tau = \frac{e}{m_{opt}^* \mu}$$

(3.3)

In the two expressions m_{opt}^* donates the electron effective mass.

Due to this effect a TCO film, that is transparent in the visible spectral range, will reflect light in the long wavelength region, with the plasma frequency roughly defining the border between the two regimes. The damping defines the steepness of the transition. As the plasma frequency shifts to higher frequencies with increasing carrier concentration, the demand for high transmission at a specific wavelength will set an upper limit for the carrier concentration, while optical transmission below the plasma frequency and conductivity will both benefit from high mobilities [34].

The Drude expression has been used by various authors to derive information on free carrier behavior in ZnO thin films by evaluation of reflection data, transmission spectra or ellipsometric spectra. However, deviations from the Drude theory can be observed if both transmission and reflection data are taken into account. The main reason is a frequency dependance of the damping frequency in highly doped TCOs for frequencies above the plasma frequency. Generally this is expressed in a frequency-dependant real part of the dynamic resistivity, ρ. It follows a power law ρ is proportional to ω^α, in which α indicates the dominant scattering behavior [34].

The theory was applied to ITO films by Hamberg et al. and showed an accurate description of the dielectric function. The theory was later also applied to ZnO thin films [34].

Unfortunately the solution of the underlying equations are challenging in terms of computation and hence difficult to implement for fitting of optical spectra. Thus other authors implemented analytic functions in order to describe the frequency dependant damping [34].

In this approach an analytic expression is used to describe the frequency dependance of the damping and $\omega_\tau(\omega)$ is expressed as;

$$\omega_\tau(\omega) = f(\omega)\omega_{\tau 0} + (1 - f(\omega))\omega_{\tau 1}\left(\frac{\omega}{\omega_{tr}}\right)^\alpha$$

(3.4)

Where;

$$f(\omega) = \frac{1}{1 + \exp\frac{\omega - \omega_{tr}}{\sigma}}$$

(3.5)

In this case the parameter $\omega_{\tau 0}$, describing the low frequency limit of the damping frequency, has to be used for calculation of carrier mobility using (3.3). ıt is reasonable to set the exponent $\alpha = -3/2$, which is characteristic for ionized impurity scattering [34].

This extended Drude approach has been used to evaluate optical transmission and reflection data in the visible and the near-infrared spectral range. The effective mass m_{opt}^* of the free carriers is derived by correlating values for plasma frequency obtained from fitting with carrier concentration determined with Hall measurements [34].

3.2 Electron Concentration

ZnO is a wide and direct band gap II–VI semiconductor and has potential applications. ZnO exhibits good piezoelectric, photoelectric and optical properties, and can be suitable for an electroluminescence device [35].

Fabrication of p-type ZnO or the formation of ZnO p–n junction is very difficult because ZnO thin film shows n-type conduction due to many native defects, such as oxygen vacancies and zinc interstitials. However, recent successes in producing p-type ZnO and ZnO p–n junction have opened up the possibility of producing blue and ultraviolet (UV) light emitters. Stoichiometric zinc oxide is an insulator that crystallizes with the wurtzite structure to form transparent needle-shaped crystals [35].
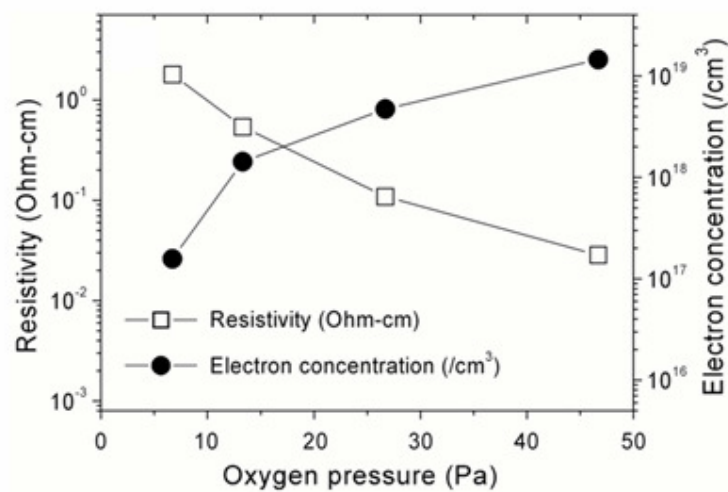
The structure contains large voids which can easily accommodate interstitial atoms. Consequently, it is virtually impossible to prepare really pure crystals; also, when these crystals are heated, they tend to lose oxygen. For these reasons, ZnO shows n-type semiconducting properties with many defects, such as the lack of oxygen and the excess of zinc. ZnO typically exhibits UV band edge emission and a broad visible band emission due to native defects [35].

The visible photoluminescence (PL) is most commonly green, though other peaks such as, for example, orange and yellow emission have also been reported. Stoichiometric ZnO thin films usually show strong UV luminescence. It is known that visible luminescence is mainly due to defects which are related to deep level emissions, such as zinc interstitials and oxygen vacancies. Recently, it was reported that the shallow donors are responsible for the pre dominantly n-type conductivity in otherwise undoped materials. However, it is not sufficient to investigate on relationship between optical properties and electrical properties [35].

Figure 3.3, below, shows the result of electron concentration and resistivity of ZnO thin film.

Results show that control of electron concentration in ZnO thin films is possible throughout oxygen partial pressure variation. Resistivity decreased as oxygen partial pressure increased [35].

Figure 3.3: Resistivity electron concentration relationship in ZnO [35].

ZnO has many native defects due to lattice structure that contains large voids which can easily accommodate interstitial atoms. These native defects in ZnO contribute the increase of n-type carrier concentration. To fabricate the p-type ZnO and other electronic devices, it is important to control the number of native defects [35].

Al^{3+} solubility limit on thin films is better confirmed, in an indirect way, from electrical measurements (film conductivity). It can be reminded that for TCOs, conductivity is directly linked to carrier concentration i.e. here, aluminium doping rate since a supplementary free electron is created upon the non-aliovalent substitution of Al^{3+} for Zn^{2+}. From conductivity measurements, several reports and seem to show that it is possible to dissolve up to 1 mol.% of Al in zinc oxide [11].

3.3 Electron Mobility

Carrier (electron) mobility is an important phenomenological parameter for describing the operation of semiconductor devices such as metal-oxide semiconductor field effect transistors and solar cells. It is one of the basic input parameters for expressing electrical current in devices. In addition the determination of doping level in wafers requires a knowledge of carrier mobility. Several techniques have been used in determining carrier mobilities in semiconductors. However, they all require samples specially prepared or when this is not the case thay require electrical contacts in signal acquisition [36].

When electrons are confined in two-dimentional (2D) materials, quantum mechanically enhanced transport phenomena, as exemplified by the quantum Hall effects (QHE), can be observed [37].

In the investigations of electrical properties of semiconductors it is usual to determine the conductivity and Hall coefficient R given by;

$$\sigma = n q \mu \tag{3.6}$$

and

$$R = \frac{1}{n q c} \cdot \frac{\mu'}{\mu} \tag{3.7}$$

Where n is the number of carriers per unit volume, c is the velocity of light in vacuum, q is the electronic charge, μ is the drift mobility of the carriers and μ' is the Hall mobility of carriers [38].

From equatins 1 and 2, we obtain;

$$\mu' = c\,R\,\sigma.$$

(3.8)

Thus, it is seen that the Hall mobility, μ' can be measured without ambiguity. To obtain the density of carriers and drift mobility a knowledge of dependence of

μ' / μ on impurity content is necessary [38].

Hall effect and magnetoresistance are far less informative than they are in crystalline materials [39].

Most III-V compound semiconductors have high electron or hole mobility when the impurity or carrier concentration is low, regardless of the doping type. In these materials, the mobility decreases gradually when the impurity concentration is above 10^{16} cm^{-3} [40].

According to Studenikin et al. [41], many papers were mostly concerned with preparation of the films and investigation of their structural, optical and electrical properties; and scanned attentions was given to the relaxation properties of ZnO films, although some reported slow relaxation processes without presenting a detailed study.On the other hand the relaxation proerties of semiconductor films are of interest both for a fundemental understanding of transport mechanisms and for testing new materials.

As Studenikin et al.[41], suggested; in many cases the specific resistivity and the Hall effect of a conducting material are measured by cutting the sample in the form of a a bar. Current contacts A and B and voltage contacts C, D, E and F are attached to the bar as shown in Figure 3.4. The specific resistivity is then derived from the potential drop between the points C and D or E and F from the dimensions of the sample. On the other hand, the Hall voltage can be measured between the points C

and E or D and F. the current contacts must be far away from the points C, D, E and F in order to ensure that the lines of flow are sufficiently parallel and are not changed on application of a magnetic field.
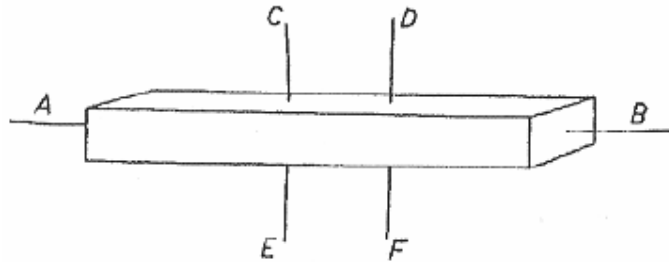
Figure 3.4 : The classical shape of a sample for measuring specific resistivity [42]

For the measurement of the specific resistivity and Hall effect of a semiconductors are more complicated shape of the sample has often to be used. A well-known example is the bridge shaped sample as shown in Figure 3.5.
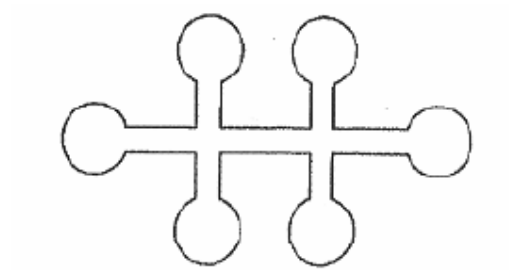
Figure 3.5: The bridge shaped sample [42]

The large areas at the ends have the task to provide low-ohmic contacs. Furthermore, when makin these contacts a heat treatment is often necessary which in this case can be done without heating that part of the sample which is under measurement [42].

It will be shown that the specific resistivity and the Hall effect of a falt sample of arbitrary shape can be measured without knowing the current pattern if the following conditions are fullfilled;

- The contacts are at the circumference of the sample
- The contacts are sufficiently small
- The sample is homogeneous in thickness
- The surface of the sample is singly connected, i.e., the sample does not have isolated holes [42].

Unlike traditional methods; Studenikin et al. [41], employed a setup (Figure 3.6) for Hall effect measurements in the dark and under illumination, which is designed and built at the University of Guelph, and the software allowed fully automated four-probe resistivity and Hall effect measurements.
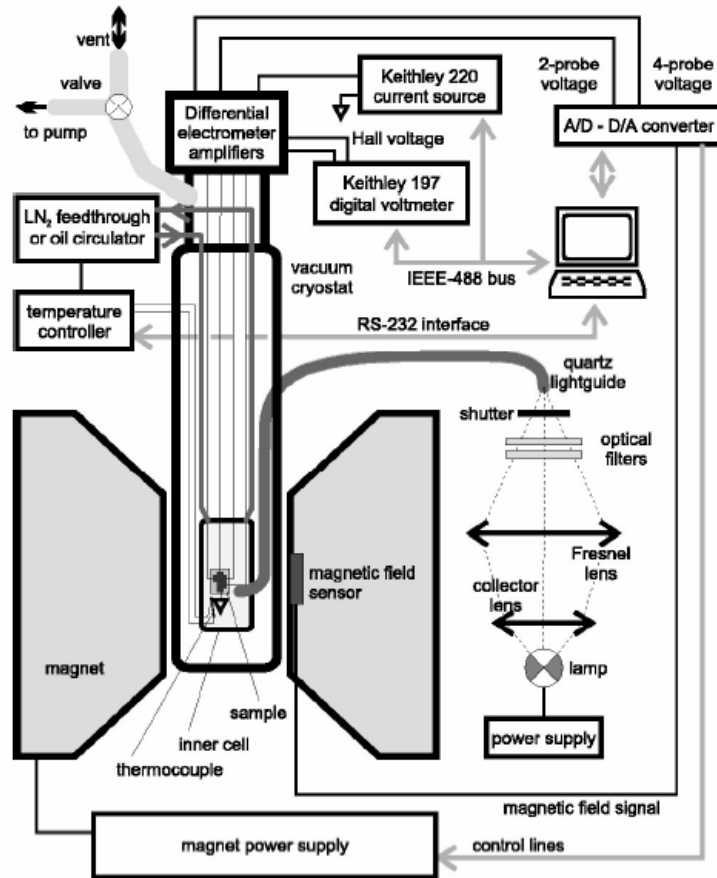
Figure 3.6: Schematic diagram of the automated Hall effect setup [41]

4. OPTICAL PROPERTIES OF AZO FILMS

Future energy supply and energy security will demand revolutionary advances in technology in order to maintain or forward today's (2007) general standard of living and economic prosperity [43].

Clearly the TCs can be viewed as ''solar energy materials'', whose properties have been given a bird's eye perspective in recent articles [22].

The applications of TCs, hence, can rely on their spectral selectivity. Other possible uses emerge from the angular properties of the radiation that surrounds us, specifically by the fact that one can take advantage of the Sun's passage over the vault of heaven to have different performances for midday and dawn or dusk. Still other applications ensue from the fact that ambient radiation or human needs vary during the day and season, so that solar energy and/or visible light ideally should be admitted or rejected as a function of time [22].

When electromagnetic radiation impinges on a material one fraction can be transmitted, a second fraction is reflected, and a third fraction is absorbed. Energy conservation yields, at each wavelength, that;

$$T(\lambda) + R(\lambda) + A(\lambda) = 1 \tag{4.1}$$

where T, R, and A denote transmittance, reflectance, and absorptance, respectively [22].

Another fundamental relation ship, also ensuing from energy conservation and referred to as Kirchhoff's Law, is;

$$A(\lambda) = E(\lambda) \tag{4.2}$$

with E being emittance, i.e., the fraction of the black body radiation that is given off at a particular wavelength. Eq. (4.1) is of practical relevance mainly for $\lambda \square 3$ µm [22].

Recently, number of researchers have focused and paid attentiaon in preparing the suitable conditions so as to obtain a good quality of ZnO thin films which affected the structural, electrical and optical properties [44].

Al-doped ZnO compounds are the most conventional transparent conductive oxides (TCOs), which are useful as transparent electrodes (opto-electronic devices) or as thermal insulator films in smart windows (low emissive windows) [11].

Substitution of aluminium for zinc remains nevertheless quite difficult because of the difference in oxidation state, ionic radius and coordination preference [11].

AZO films have been prepared by various thin-film deposition techniques, including magnetron sputtering , spray pyrolysis, chemical vapor deposition, pulsed laser deposition, reactive electron beam evaporation and sol–gel process, etc. Recently, a high-quality AZO film prepared by radio-frequency magnetron sputtering has been used as an anode. The film exhibited a resistivity of 7.5×10^{-4} Ω-cm and an optical transmittance over 85% in the visible spectral region. [17].

According to S. Fernandez et al. [45], for most applications high transmission in the visible range is very important. Due to the fact that many researhes based on results from visible range.

The analysis of optical transmission spectra is one of the most productive tools for understanding and developing the band syructure and energy band gap, E_g, of crystalline structure [46].

The transmittance of the uncoated glass substrate is greater than 93% over the entire spectrum region, except for wavelengths below 1000 nm a slight increase of transmission of about 95% is observed; in fact, this is due to the light scattering by the bubbles (imperfection) inside the substrate [47].

The spectrum can be roughly divided into two regions:

- A transparent region with the interface pattern
- A strong absorption range in the UV range.

In the region of low absorption, the incident light traverses and reflects in the film several times and produces the interference fringes [46].

5. RADIATION EFFECT

Interactions between radiation and material can be grouped into two broad classes:

1. Those concerning radiochemistry (i.e., ionization and free radical production)
2. Atomic displacement collisions in ordered solids.

Theoretical calculations of the magnitudes of these interactions are somewhat imperfect; undercertainties arisee from the inability of investigators to determine accurately the damage mechanism and the influence of material impurities and environmental conditions on the radiation effect [48].

Literature on engineering tests of radiation effects on the properties of structural materials is extensive, but these tests seldom duplicate the exact materials used in spacecraft or the actual conditions of the space environment. In some circumstances, these differences can be critical [48].

In general, mechanical properties of structural metals or ceramics will not be significantly degraded following exposure to fluences of $\square 10^{17}/cm^2$ protons (E$\square$1 MeV), $\square 10^{17}/cm^2$ neutrons (E $\square$ 1 keV), or $\square 10^{18}/cm^2$ electrons (E$\square$1 MeV). It is expected, therefore, that space radiation will not constitute a significant hazard because such fluences can be accumulated only on extremely long missions (hundreds of years) [48].

Polymeric substances, however, are considerably more sensitive to radiation and significant effects are to be expected. In the case of all three categories of materials (metals, ceramics and polymers) nuclear-reactor and radio-isotope power radiations are of more immediate concern than space radiation because of the high radiation-dose rates associated with these internal sources [48].

Solar irradiation is dependent on different causes including astronomical and meteorological factors. In practical studies it is not possible to consider all the factors, and therefore, so far simple but effective models for its prediction from a few numbers of factors are presented. The first of such models takes into consideration only the sunshine duration measurements for the solar irradiation estimation, and unfortunately, it is still under use without critical assessment of the underlying restrictive assumptions and simplifications in model parameter estimation methodology [49].

Energetic particles and photons can interact with solids to produce atomic displacements, electronic excitations, or both. Atomic displacements result from the elastic scattering of an energetic particle by an atomic nucleus so that the kinetic energy transferred to the nucleus in the collision is sufficient to break the chemical bond to neighboring atoms. The moving atom may then serve as a projectile to produce secondary displacements or, if sufficiently energetic, will ionize or otherwise excite other atoms adjacent to its path [48].

Electron-induced displacement damage in materials is qualitatively and quantitatively unlike that caused by protons or alpha particles, and neutrons produce microscopic modifications in the properties of solids that are dissimilar to those caused by the other particles. A crucial point in this regard is the effectiveness of thermal annealing in restoring the preirradiation mechanical properties of metals. Neutron-irradiated metals generally tend to retain some remnants of radiation damage, even after thermal treatment at elevated temperatures (875 °K), but electron-induced damage is observed to anneal usually below 300 °K [48].

Electronic excitation is produced directly by electron, gamma, proton, or ion irradiations; however, fast neutron irradiations can also produce electronic excitation. When a neutron-produced displaced atom is accelerated to a speed exceeding that of an electron in its outermost shell, the atom will tend to lose electrons and appear as a rapidly moving ion. In hydrogeneous substances and other materials having low atomic numbers, electronic excitation by neutrons is quite significant [48].

5.1 Types of Radiation and Ionizing Radioation

Ionizing radiation is energy that is carried by any of several types of particles and rays (electromagnetic radiation) given off by radioactive material, X-ray machines, and nuclear reactions. This energy can knock electrons out of molecules with which they interact and thus, creating ions. Non-ionizing radiation such as that emitted by a laser, is different because it does not create ions when it interacts with but dissipates energy generally in the form of heat. The three main types of ionizing radiation are alpha particles, beta particles and gamma rays [50].

An alpha particle consists of two protons and two neutrons and is identical to the nucleus of helium atom.because of its relatively large mass and charge, an alpha particle produces ions in a very localized area. An alpha particle loses some of its energy each time it produces an ion (its positive charge pulls electrons away from atoms in its path), finally aquiring two electrons from an atom at the end of its path to become a complete helium atom. An alpha particle has a short range (several centimeters) in air and it can not penetrate the outer layer of skin [50].

Beta particles can be either negative (negatron) or positive (positron). Negatrons are identical to electrons and originate in the nucleus of an atom that undergoes radioactive decay by changing neutron into a proton. The only difference between a negative beta particle and an electron is the ancestry. A beta particle originates in the nucleus whereas an electron is external to the nucleus. Unless otherwise specified, the term "beta particle" generally refers to a negatron. A positron is emitted from an atom that decays by changing a proton into a neutron. Beta particles are smaller and more penetrating than alpha particles, but their range in tissue is still quite limited. When its energy is spent a negatron attaches itself to an atom and becomes an ordinary electron, while a positron collides with an ambient electron and the two particles annihilate each other producing two gamma rays. When a negatron passes close to the nucleus of an atom, the strong attractive Coulomb force causes the beta particle to deviate sharply and lose energy at a rate proportional to the square of the

acceleration. This energy manifests itself as photons termed Bremsstrahlung. The amount of beta energy converted into photons is proprtional to the enery of the beta particle. This effect is only significant for high-energy beta particles generally passing through very dense materials such as lead, i.e., those with higher atomic numbers and so more photons in the nucleus [50].

Gamma rays are electromagnetic radiation given off by an atom as a means of releasing excess energy. They are bundles (quanta) of energy that have no charge or mass and can travel long distances through air (up to several hundred meters), body tissue and other materials. A gamma ray can pass through a body without hitting anything, or it may hit an atom and give that atom all or part of its energy. This normally knocks an electron out of the atom, ionizing it. This electron then uses the energy it receives from the gamma ray to create additional ions by knocking electrons out of other atoms. Because a gamma ray is pure energy, it no longer exists once it loses all its energy. The capability of a gamma ray to do damage is a function of its energy, where the distance between ionizing events is large on the scale of the nucleus of a cell [50].

Additional forms of ionizing radiation beyond the three types in Figure 5.1 include neutrons, protons, neutrinos, muons, pions, heavy charged particles, X-rays and others. essentially all radioactive materials at the Hanford Site originated from neutron interactions with uranium fuel to produce plutonium. By products of this process include fission products (most of which are in the high-level waste currently in on site storage), activation products in the containment and reactor coolant materials, and various radioactive wastes [50].
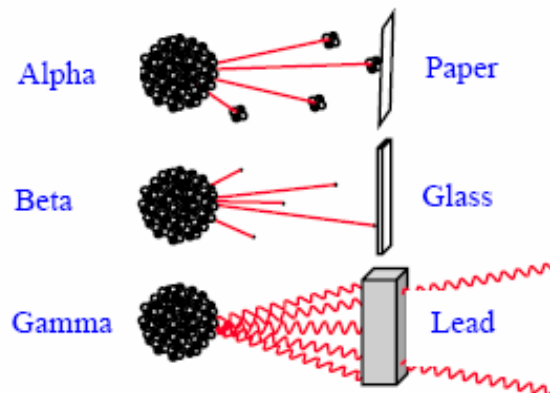
Figure 5.1: Three types of ionizing radiation [50].

Ionization effects can be studied by exposing materials to gamma ray sources (cobalt-60 or cesium-137) or by exposure to a charged particle accelerator beam. In most of the radioisotope facilities, it is a reasonable simple method to control atmosphere, temperature and pressure in the vicinity of specimens. On the other hand ingenuity is required to achieve cryogenic temperatures for samples exposed to the output of low energy (1 MeV or less) particles accelerators [48].

Isotopes are different forms of an element that have the same number of protons in the nucleus but a different number of neutrons. There are nine major radioactive cobalt isotopes. Of these, only cobalt-57 and cobalt-60 have half lives long enough to warrant concern. The half laves of all other isotopes are less than 80 days. Cobalt-57 decays with a half life of 270 days by electron capture and cobalt-60 decays with a half life of 5.3 years byemitting a beta particle with two energetic gama arays; the combined energy of these two gamma rays is 2.5 MeV (one has a energy of 1.2 MeV and the other has an energy of 1.3 Mev) [50].

The properties of cobalt-60 are shown in Table 5.1.

Table 5.1: The properties of cobalt-60 [51].

Radioisotop	K_γ (R m² / Ci h)	A (Ci)	$T_{1/2}$ (y)	E_γ (MeV)	Abundance (%)	Production Mode
Co-60	1.32	0.018021	5.27	1.17	99.90	Co-59 (n,γ)
				1.33	99.98	

5.2 Effect of Radiation on Materials

All organisms are being exposed to ionizing radiation from natural sources all the time. Radiation doses are typically given in units of rem or millirem (mrem), which is one-thousandth of rem. This unit was developed to allow for the consistent reporting of hazards associated with the various types and energies of radiation on the human body. The rem is the product of the absorbed dose in rads (i.e., the amount of energy imparted to tissue by the radiation, where 1 rad equals 0.01 joules/kg) and factors for the relative biological effectiveness (RBE) of the radiation. The RBE is directly related to the linear energy transfer (LET) or distance over which the radiation energy is imparted to the absorbing medium and is accounted for by a quality factor. For example, alpha particles are 20 times more hazardous than beta particles for the same energy deposition and hence have a quality factor of 20, whereas the quality factor for beta particles is one [50].

Materials for which the effect of radiation shall be determined shall include, but not be limited to all metals, alloys, polymers, ceramics, graphite, glasses and thermal control coatings [48].

Analysis of structural parts shall, as a minimum, account for radiation-induced modifications to tensile-yield strength, ultimate tensile strength, shear strengh, ductility, ductility-to-brittle transition temperature, fatigue strength, fracture toughness, hardness, creep, stress rupture, burst strength, impact resistance and compressive strength as applicable. The analysis shall be used on data showing the nature and magnitude of modifications to these properties for materials either identical or similar to those being analyzed. The radiations and other environmental conditions such as temperature and the pressure and composition of ambient gases shall be as nearly identical to those expected to be encountered as is practicable [48].

Analysis of insulating materials shall as a minimum account for radiation-induced modifications to thermal conductivity [48].

Analysis of heat shield and ablative materials shall as a minimum account for radiation induced modifications to specific heat, thermal conductivity, stored energy, heat of fusion, and heat of sublimation [48].

Analysis of thermal control surfaces and coatings shall as a minimum account for changes in optical absorptance, reflectance and emmittance resulting from exposure to radiation. The analysis shall be based on data showing the nature and magnitude of modifications to these properties for materials either identical or similar to those being analyzed, under radiations as nearly identical to those expected to be encountered as is practicable, and either identical or similar environmental conditions such as temperature and the pressure and composition of ambient gases [48].

Candidate materials for each structural function should be rated for relative radiation hardness. The preliminary evaluation should include:

1. Tabulation of the minimum acceptable engineering properties of interest for each part.
2. Enumeration of the available materials whose initials (i.e., unirradiated) properties meet the minimum acceptable engineering requirements for that part.
3. Review of the existing compilations of radiation effects in various materials and a determination of the radiation level at which the engineering properties fall below minimum acceptable values.
4. Elimination from consideration those materials for which there is clear evidence of failure at the predicted level of exposure [48].

If the material does not meet the required radiation hardness level, alternate designs should be considered [48].

Absorption of neutron and gamma radiation can cause temperature increases in syructural members, heating effects should be computed [48].

Polymers are the structural materials most seriously affected bu radiation. The role of temperature, pressure and composition of the projected environment should be taken into account when acceptability of polymers in a radiation environment of more than 10^5 rad (material) has been determined by analysis [48].

Ceramic properties appreciably affected by neutron irradiation include density, elastic modulus, compressive strength, mechanical integrity and thermal conductivity. Fast neutron (E $\square$1keV) effects are significant at levels near 5 x 10^{18} n/cm^2. The effects of gamma rays or charged particles should always be taken into consideration when the dose exceeds 10^6 rad (material) [48].

The principal structural properties of graphite that may be significantly modified by radiation include density, thermal conductivity, and stored energy. Changes in these properties should be accounted for when fast-neutron (E $\square$1keV) fluences are in excess of 10^{19} n/cm^2 [48].

Structural properties of glass are usually unaffected by fast-neutron (E $\square$1keV) fluencesless than 10^{19} n/cm^2. When the glass is to be used as a viewing port, darkening of the glass by ionizing radiation usually limits its usefulness. Under such circumtances it is advisible to specify radiation-resistant glass [48].

Figure 5.3 shows unirradiated and irradiated AZO samples.
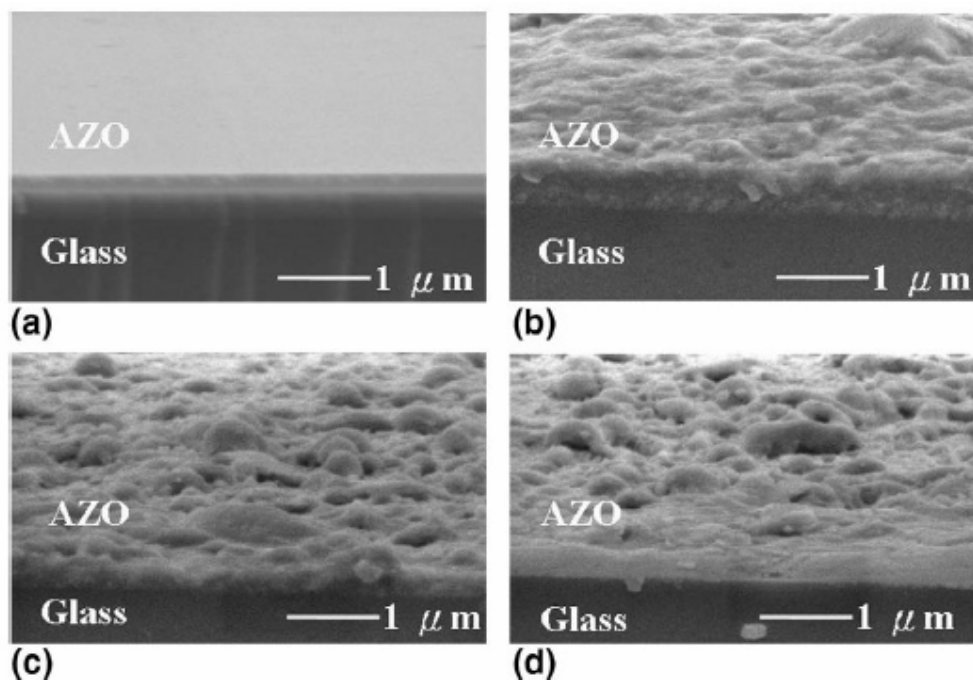
Figure 5.3: SEM images of AZO films a) before and b-d)after irradiation with 1,3 and 5 laser shots with E$_L$:250 mJ, respectively [17].
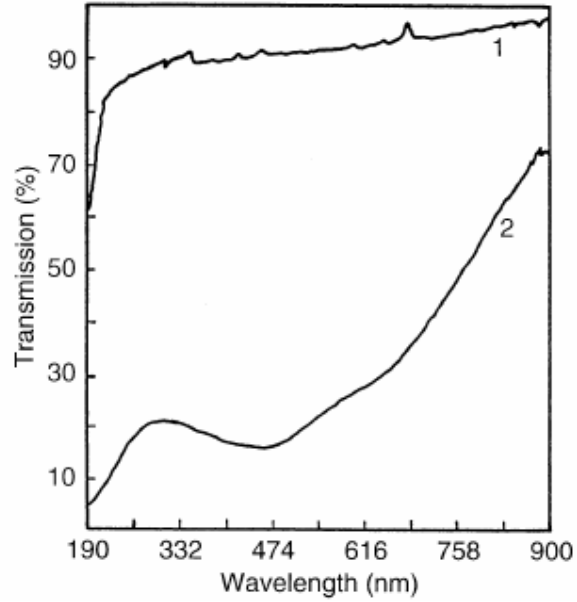
Figure 5.4: Optical absorption spectra of natural quartz measured before (1) and after
g- irradiation (2) [52].

According to Limoeiro et al. [52], recently, in the course of gamma-ray and electron
beam irradiation to gelatin aqueous solutions, it is observed that the light scattering
intensity of dilute solutions of the irradiated gelatin was significantly stronger than
that before the irradiation (Figure 5.4).

6. EXPERIMENTAL

This study focuses on the optical and electrical properties of Al doped and undoped ZnO thin films which are produced by dip coating via sol-gel process. In this respect, AZO and ZnO thin films are deposited on substrates homogeneously and final samples are examined under spectrophotometry for optical and four point probe for resistivity measurements.

6.1 Substrate Preparation

In this study, as the substrate materials, soda-lime silica glass was utilized for investigation of optical properties and Corning 7059 glass was used for electrical resistivity evaluation.

It is suitable to include some information on substrate materials for coatings of TCs. From the viewpoint of practical use, however, the films should be deposited on an amorphous substrate such as glass substrates. It can exhibit a variety of properties [22,53].

Soda-lime silica glasses were cut in dimentions of 25x40 mm. Corning glasses were ready to use, which were 25x25 mm in dimensions.

Both soda-lime silica and Corning glasses are cleaned in the same procedure, shown in Figure 6.1.
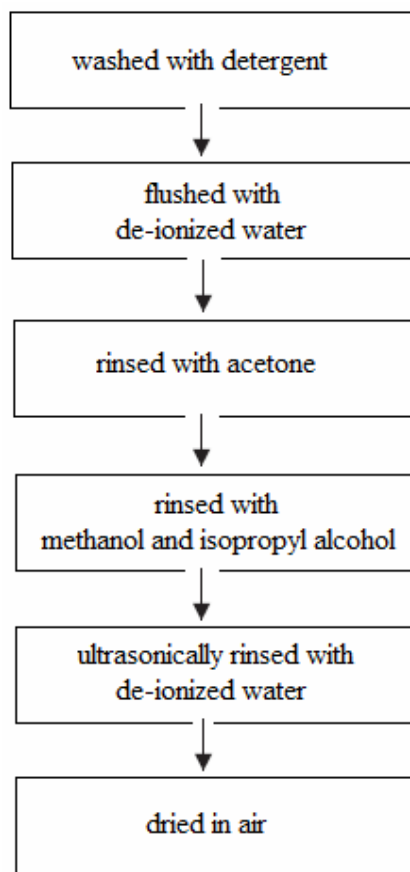
Figure 6.1: The flow chart showing the procedure for cleaning substrates

After preparation of glasses; it is carefully taken into account that glasses were placed to cleaned boxes if they were not going to be used on that time.

For ultrasonic cleaning Sonorex Ultrasonic Bath RK-100 H is utilized (Figure 6.2).

Figure 6.2: Ultrasonic Bath Equipment [54].

6.2 Preparation of Precursor Solution

Three sol-gel categories have been used to deposit zinc oxide thin films ;

  i.   Processes based on the use of undoped ZnO.

 ii.   Processes based on the use of undoped ZnO with addition of distilled water into solution of zinc oxide.

iii.   Processes based on the use of doped ZnO and acquiring AZO compound.

A solution of ZnO precursor was made by dissolving zinc acetate dihydrate [$Zn(CH_3CO_2)_2.2H_2O$] in ethanol.

The stability of the process was set by control of the hydrolysis and condensation reactions such that they take place only when the solution dries, solvent is lost or temperature is elevated [10].

Therefore, the diethanolamine (DEA) was added as a chelating ligands to improve the precursor solubility. The optimum amount of additive in the system provided a homogeneous distribution of the metal ions and prevented their precipitation from the solution prior to thermal treatment. The molar ratio of DEA/zinc acetate was 1:1.

The solution then hydrolized in (ii) and (iii) with 2 mol H_2O per mol metal acetate to improve the wetness and uniformity of the coating on the substrate [10].

To obtain aluminum doping, aluminum nitrate nanohydrate [$Al(NO_3)_3.9H_2O$] was added to the solution for process (iii).

In our experiment, the dopant level, determined by 100 x [Al]/ [Al+Zn], was 3, 5, 7, 10, 20, 30, 50 mol %.

The sol was stirred at 480 (1 / min) in magnetic stirrer at 90 °C for an hour. Therefore it can be obtained the clear sol. served as the coating solution after cooling down to room temperature. The coating was usually made 3 days after the solution was prepared.

The glasses were coated after preparing the solutions having compounds and amounts shown in Table 6.1.

Table 6.1: Compounds and their amounts in solution

Compounds	Amounts		
	i	ii	iii
$[Zn(CH_3CO_2)_2.2H_2O]$	1.5364 g	1.5364 g	1.5364 g
Ethanol	50 ml	50 ml	50 ml
Diethanolamine (DEA)	0.669 ml	0.669 ml	0.669 ml
De-ionized Water	-	3 ml	3 ml
$[Al(NO_3)_3.9H_2O]$	-	-	1-50 %
			0.8-1.6 %

6.3 Depositing Thin Films

AZO thin films were deposited by dip coating the stock solution onto substrates (both on thin commercial soda-lime silica glass cover for a microslide and Corning 7059).

Cut, prepared and cleaned glass substrates were dip coated under atmospheric conditions, at about 22-25°C and 35-40% humidity.

During this process computer controlled KSVLMX2 Dip Coater equipment was utilized (Figure 6.3). Glasses are dipped into the emulsion with a speed of 200 mm/min and pulled off with a speed of 50 mm/min without holding in the sol.

After one layer is obtained on the substrate, the films were dried at 100°C, 400°C for soda-lime silica and Corning glasses, respectively, in Nabertherm furnace for 10 min. Final annealing was conducted in a temperature range of 100 to 500 °C for soda-lime silica and 700°C for Corning glasses.

In order to observe the effects of annealing conditions on resistivity four of eight samples,which are coded as I, II, III and IV, are annealed in vacuum and rest of them, which are coded as V, VI, VII and VIII, are annealed in argon ambient.
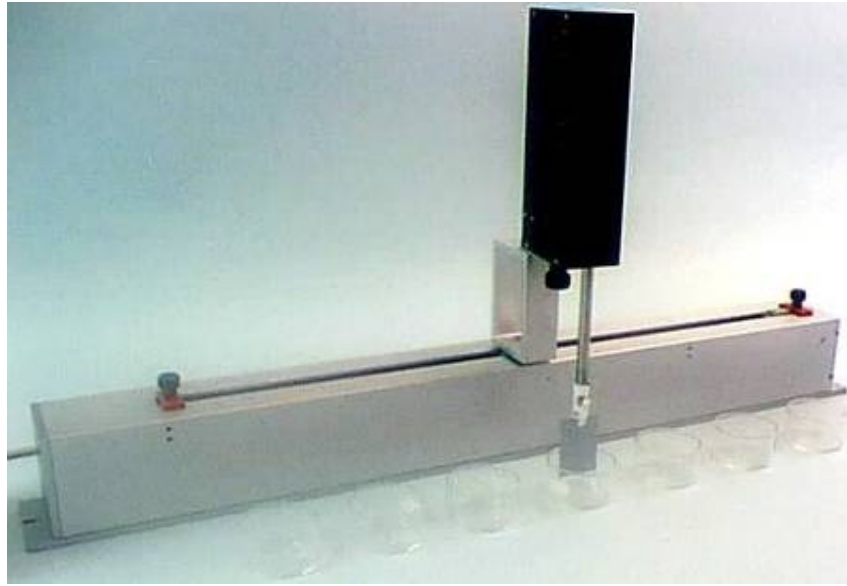
Figure 6.3: Dip Coating Equipment [55].

6.4 Irradiation Process

In order to examine the effect of gamma irradiation, Co-60 radioisotope was utilised. Co-60 radioisotope is an appropriate irradiation source for the industrial usage to obtain the photons with high energy.

Co-60 radioisotope as a gamma source emits the photons with two different energies (1.17 MeV and 1.33 MeV) and it provides gamma rays of average energy of 1.25 MeV by assuming a monochromatic 1.25 MeV source. Therefore, Co-60 radioisotope was used as gamma source to irradiate the ZnO and AZO thin films with high energy gamma rays. The activity of Co-60 was 0.018021 Ci. The absorbed dose of ZnO and AZO thin films were 0. 38 Gy.

All irradiation tests are done at room temperature.

The Co 60 radioisotope which was used during irradiation process and placement of samples around the isotope are shown in Figure 6.4. Radioisotope was placed in the middle of the circle.

(a)   (b)
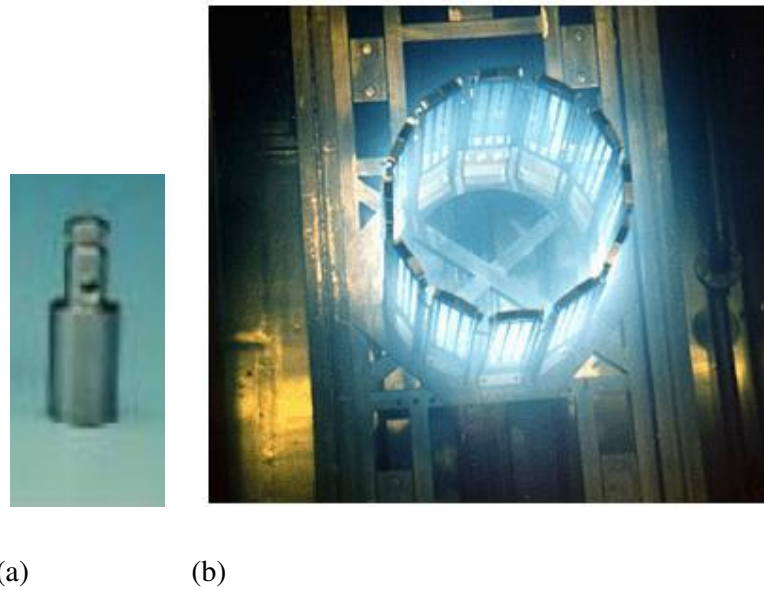
Figure 6.4: Schematic diagram of (a) Co 60 radioisotope and (b) placement of samples [56].

6.5 Characterization Tests

The characterization of the films, acquired on the surfaces of glasses, deposited by solgel technique is accomplished by;

- Transition element examination by XRF,
- Microscopic examination by SEM,
- Thickness measurement by profilometer,
- Optical properties by spectrophotometer,
- Electrical properties by using four point probe.

6.5.1 Elemental Analysis

The transition elements of soda-lime silica glass influences the colour owing to the absorption of sunlight at the color centers [57], transition elements of the soda-lime silica glass utilised in this study was examined by Innov-X XRF Analyzer, shown in Figure 6.5.

Figure 6.5: Schematic diagram of Innov-X XRF Analyzer [58].

6.5.2 Microscopic Examination

The surface morphology of the thin films was observed by using EDX equipped JEOL JSM-7000F SEM at magnification of 7500.

6.5.3 Thickness Measurement

Thicknesses of thin films are measured by using Veeco Dektak 6M Stylus profilometer, shown in Figure 6.6.

In order to measure the thickness, only half of the glasses were coated in every step. Thickness measurement is acquired from the coated to the uncoated part of the glass with a measurement interval of 6.5 um and under 8 mg load.

Figure 6.6: Schematic diagram of Veeco Dektak 6M Stylus profilometer [59].

6.5.4 Optical Properties

The optical properties of films were examined with a Lambda 950 Perkin Elmer, double beam spectrophotometer in the ultraviolet-visible-near infrared (UV/VIS/NIR) regions in the wavelength range of 280-2400 nm. Regions can be adjusted as required. (Figure 6.7).

As S.-Y. Kuo et al. [60] suggested, high transparency is the most important factor in the application of ZnO:Al films to TCOs, the optical transmittance was determined within the wavelength from 280-2400 nm.

Transmittance, reflectance, absorbance and OD (optical density) are evaluated from the values obtained from spectrophotometer by using Equation (5.1),

$$OD = \alpha t \log_{10} e - \log_{10}(1-\rho)^2$$

(5.1)

Where; t is the film thickness; α is the absorbance and ρ is the reflectance.

Also, optical bend gaps are determined from the graphs.
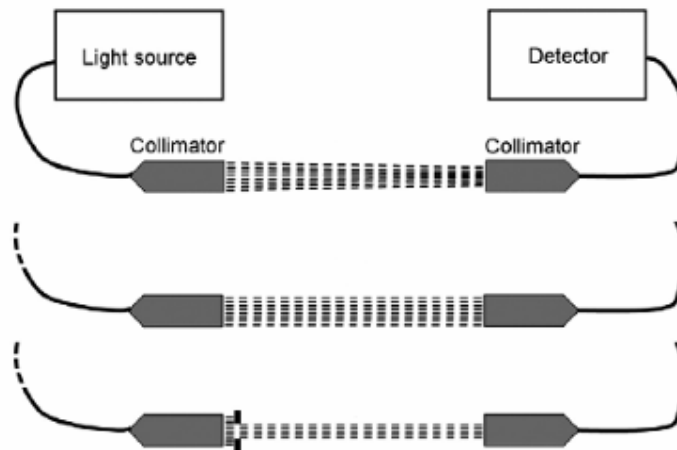
Figure 6.7: Schematic diagram of Lambda 950 Perkin Elmer [61].

6.3.4 Resistivity Properties of Films

The four point electrical probe is a very versatile device used widely in physics for the investigation of electrical phenomena.

In this study, resistivity of the samples are evaluated by four point probe from three or more different points from each samples, then average value for resistivity is calculated.

7. RESULTS AND DISCUSSIONS

7.1 Elemental Analysis

In the present study soda-lime silica glass was utilized as the substrate material. The characteristic optical density bands are explained the causes of color due to the absorption of sunlight at the color centers of the transition elements in soda-lime silica glass such as Fe and Zr at the substrate, after the gamma irradiation transition elements of the soda-lime silica glass utilised in this study was examined by Innov-X XRF Analyzer. The results of XRF measurements are given in Table 1.

Table 7.1: Transition elements of the examined soda-lime silicate substrate.

Elements	wt. %
Fe	0,09+/-0,01
Zr	0,02+/-0,00

7.2 Microscopic Analysis

In the scope of the present study; glasses were dip-coated homogeneously with different dopant concentrations, and postheated at different temperatures, between 100°C – 550°C and 400°C - 700°C, for optical and electrical properties, respectively.

Scanning electron microscopic examinations revealed that, the substrates were homogenously covered by Al doped ZnO film after sol-gel process. In Figure 7.1; the scanning electron microscopic image of the AZO thin film annealed at 400°C shows the homogeneity and accomplished wetting.
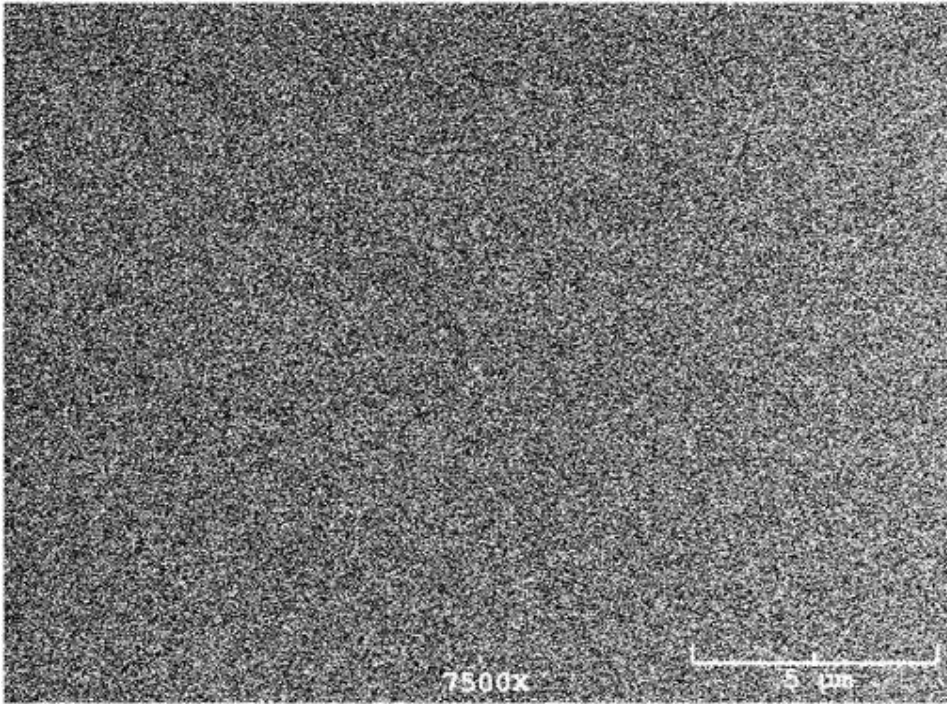
Figure 7.1: SEM image AZO film postheated at 400 ℃.
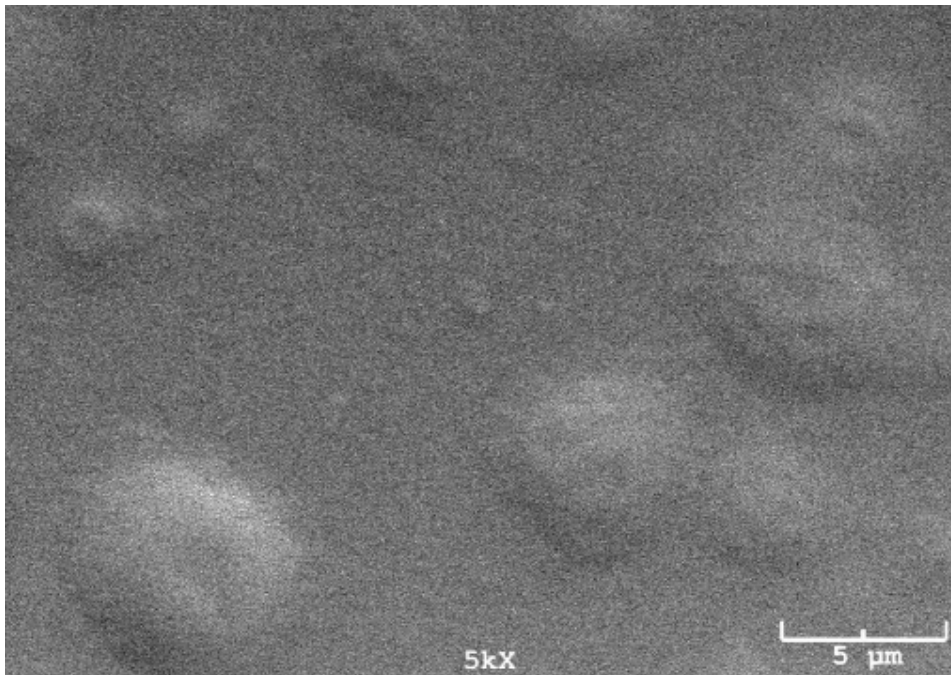
Figure 7.2: SEM image AZO film postheated at 400 ℃

It is also seen that with a high dipping rate; bubbles formation occurs and bubbles can not be eliminated during postheating. This causes a catastrophic decrease in quality of the optical properties. Figure 7.2 shows an SEM image of AZO coated surface with the inclusion of bubbles.

It is also observed that if substrate cleaning was unsuccessful before dipcoating; final surface qualities are also affected. In Figure 7.3 dirt caused, non uniform, surface is detected.
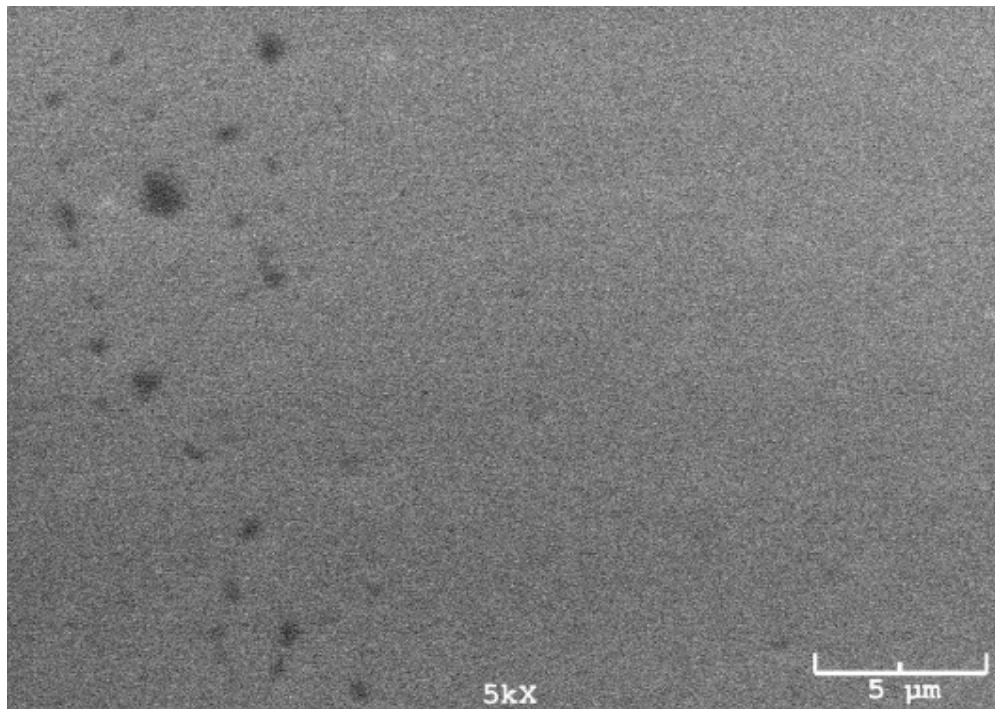
Figure 7.3: SEM image AZO film postheated at 400 °C

7.3 Optical Properties

In this study, for optical properties; results of the experiments were evaluated in three sections, in order to analyse;

i.   The effect of de-ionized water addition
ii. The effect of Al concentration present in the ZnO emulsion
iii. The effect of irradiation exposure on deposited ZnO and AZO thin films.

The Effect of The De-Ionized Water Addition

For the examined undoped and Al-doped zinc oxide based thin films, deposited on soda-lime silica glass substrates; it is reported that addition of de-ionized water to solutions increases the wetness and uniformity of the coating on the substrate according to Radhouane Bel Hadj Tahar [10] .

Figure 7.4 shows the transmittance change in undoped zinc oxide coatings, with the addition of de-ionized water, at two different post heated temperatures.

(a)
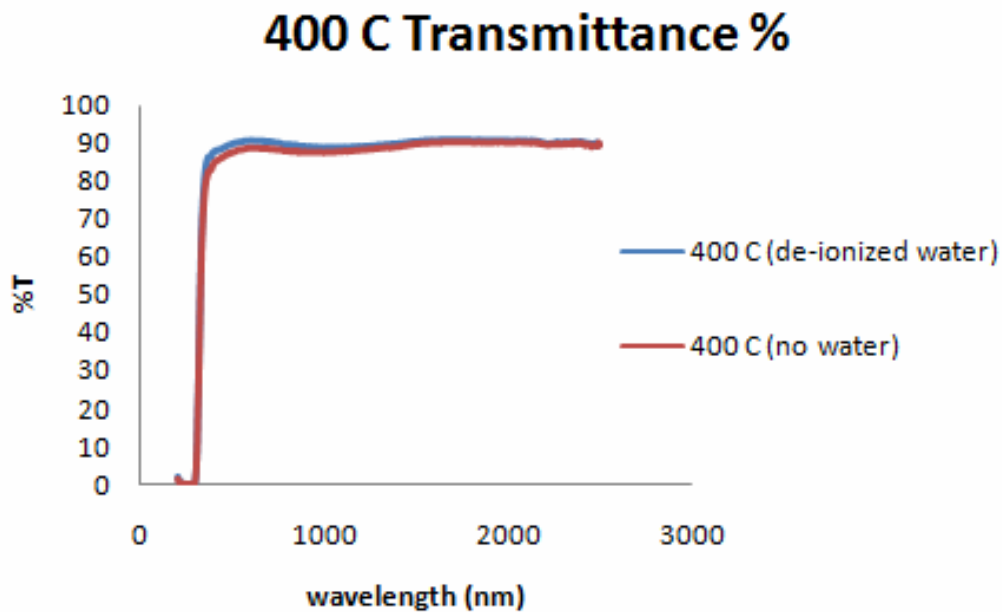
500 C Transmittance %
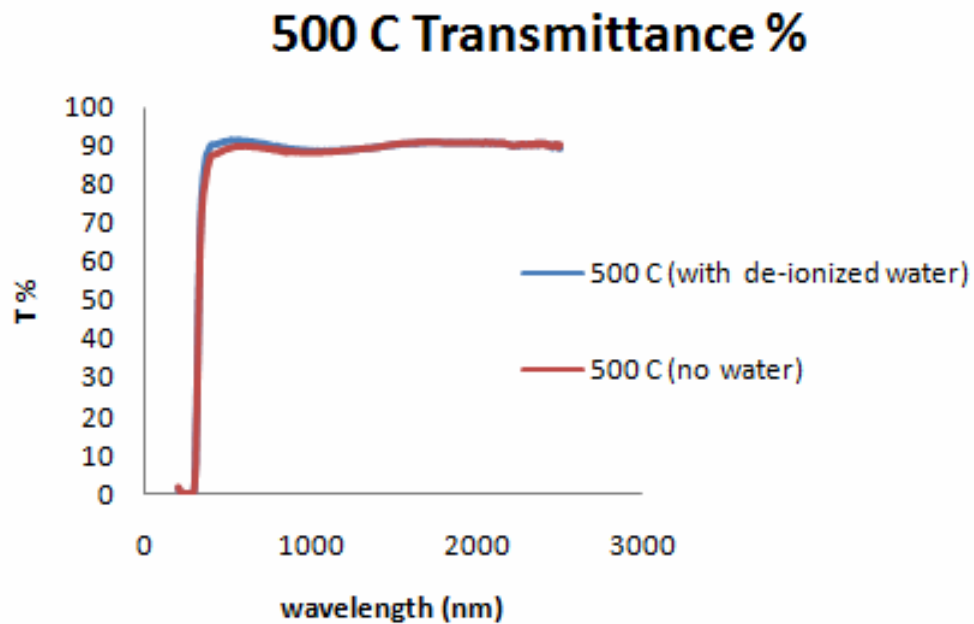
(b)

Figure 7.4: Effect of De-Ionized Water To Transmittance In Zinc Oxide Coatings at (a) 400°C and (b) 500°C.

The transmittance values are detected by 950 Perkin Elmer, double beam spectrophotometer in the ultraviolet-visible-near infrared (UV/VIS/NIR) regions in the wavelength range of 280-2400 nm.

In Figure 7.4; when blue lines, which indicate the coatings with de-ionized water, is compared to red lines, which contains no water, it is seen that there is an increament in transmittance values which means better uniformity between the substrates and coatings at both different post heating temperatures.

The Effect of Al Concentration Present In The ZnO Emulsion

This part of the work focused on the optical properties influenced by dopants. The influences of dopant concentration on the structural and optical properties were investigated. Appropriate amounts of aluminum doping were achieved by adding aluminum nitrate to the precursor solution. In this experiment, the dopant level was determined by;

100 x (Al) / (Al+Zn)   **(7.1)**

By utilization of Equation 7.1; dopant levels were 1, 3, 5, 7, 10, 20, 30, 50 mol %. The effect of dopant concentration on transmittance at 200°C, 300°C, 400°C, 500°C and 550°C are shown in Figure 7.5.

(a)

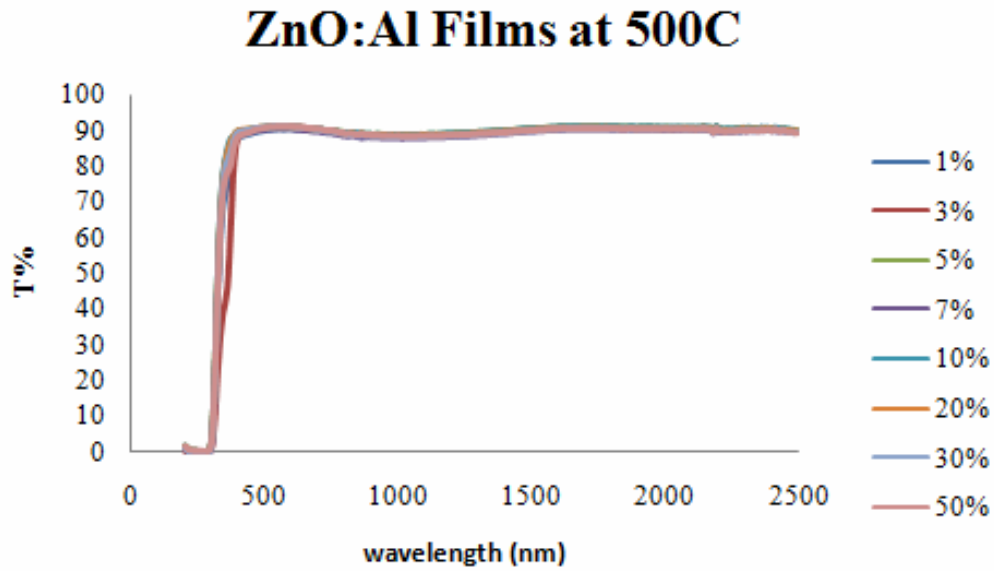(b)

(c)

ZnO:Al Films at 500C
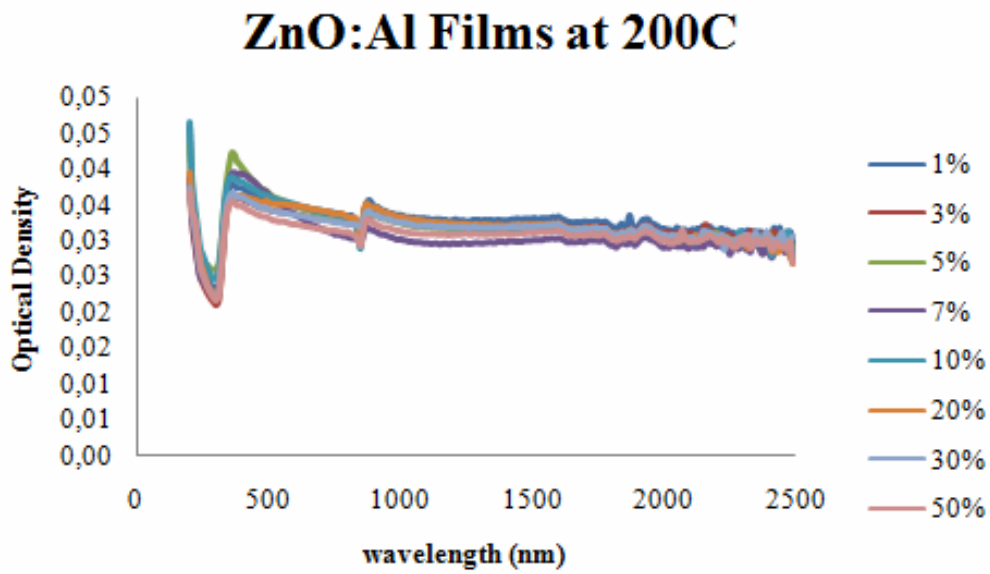
(d)

ZnO:Al Films at 550C

(e)
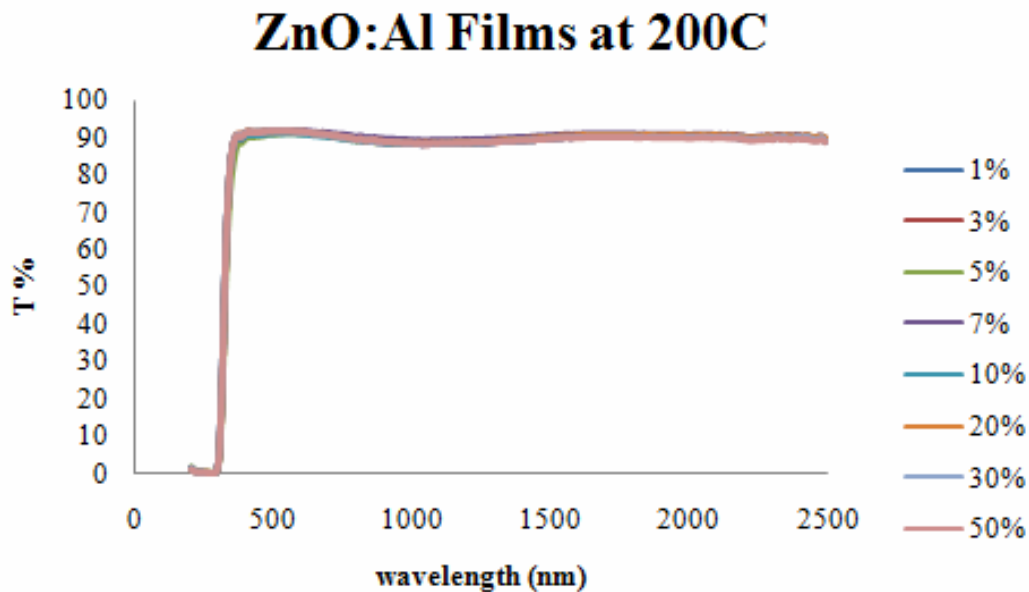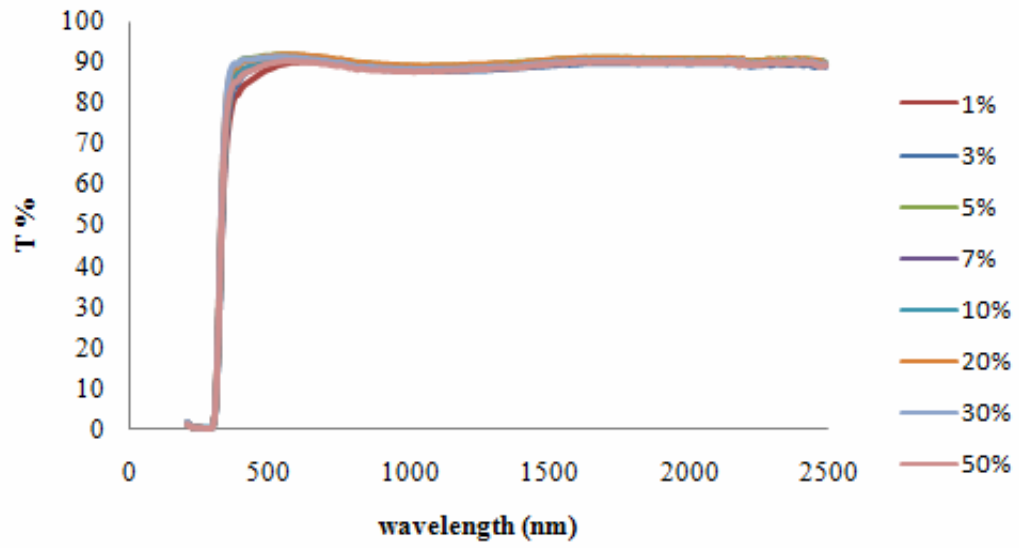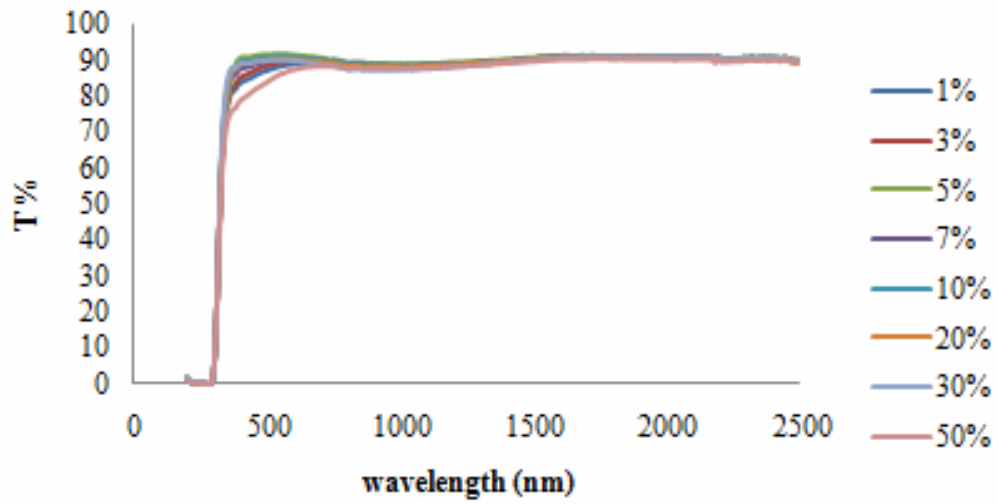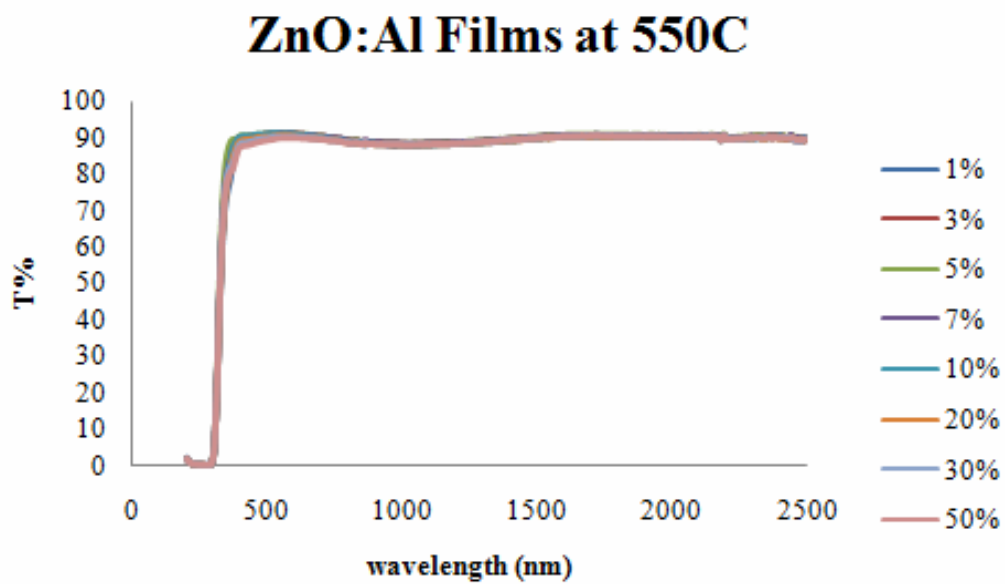
Figure 7.5: Effect of dopant concentration over transmittance % values at (a) 200°, (b) 300°C, (c) 400°C, (d) 500°C and (e) 550°C postheating temperatures

It is seen from Figure 7.5 (c) that the required properties can be obtained from postheating at 400°C. According to Shinobu Fujihara et al. [62] Generally, the thermal decomposition behavior of the precursor gel is complicated especially with various kinds of organic molecules contained (7.1). The decomposition involves many thermal effects. The gradual weight loss observed at temperatures between 172 and 445°C with a step at 353°C indicates the continual release of the organic molecules. The exotherm beginning at 250°C may be due to the combustion of the organic molecules and/or crystallization of ZnO. Due to the fact that almost all experiment results are commented on 300°C - 400°C - 500°C and 550°C.

$$Zn_2(ea)_2 \cdot (CH_3COO)_2 \rightarrow 2ZnO + \text{gaseous phases}$$

(7.2)
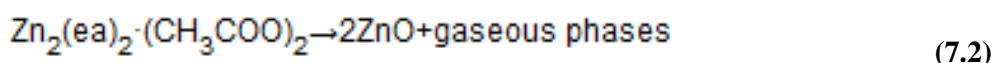
Raghvendra et al. [63] reported that absorption range of ZnO films vary in between 354 - 384 nm depending on the composition. Absorption of ZnO film at 354 nm corresponds to the band gap for 3.5 eV and absorption at 384 nm corresponds to the band gap for 3.23. eV. On the other hand, optical density band between ~ 380 and 460 nm can be attributed to the presence of ferritic iron (Fe^{+3}) and zirconium in the composition of the substrate (Table 1). Zirconium shows broad absorption feature between ~ 230 nm and 400 nm. Fe^{+2} ions give the absorbption band at approximately 1000 nm depending on the composition of material. The particular band character of Fe^{2+} in terms of shape, intensity and wavelength position varies with glass composition. The wavelength position of Fe^{2+} changes between 900–1300 nm depending on the glass composition [64,65]. Therefore the optical density bands determined by Figure 7.6 can be associated with the transition element content of the substrate (Table 1). The enhancement of colour by Zn in ZnO film and by Fe and Zr in the substrate can be explained by means of the created colour centres at the certain optical density bands.

The effect of dopant concentration on optical density at 200°C, 300°C, 400°C, 500°C and 550°C are shown in Figure 7.6.
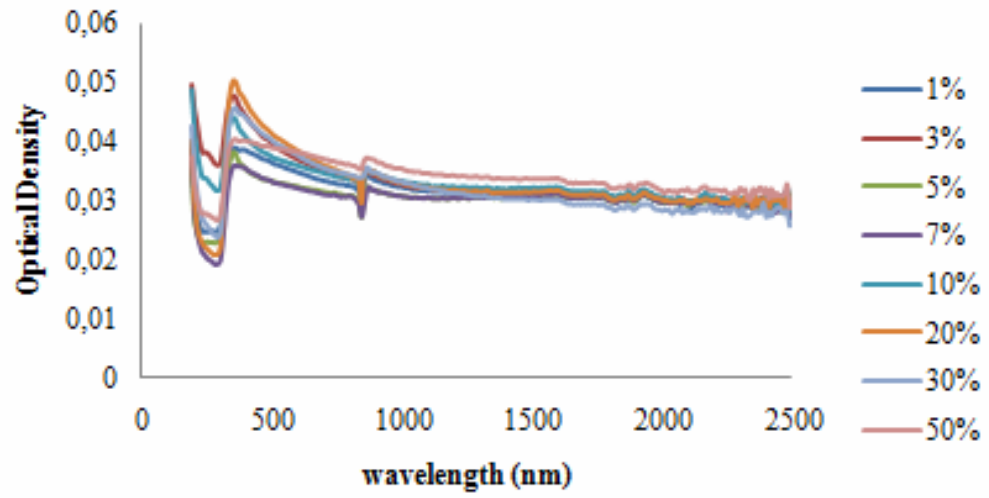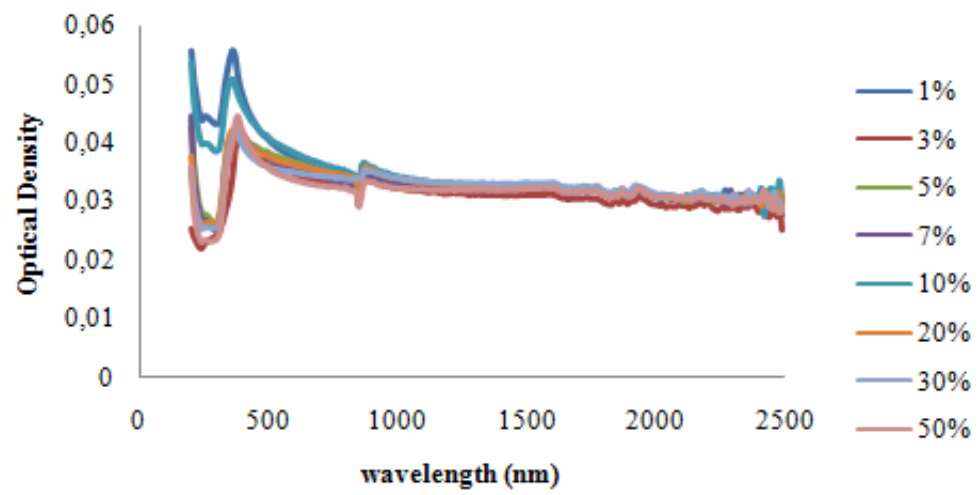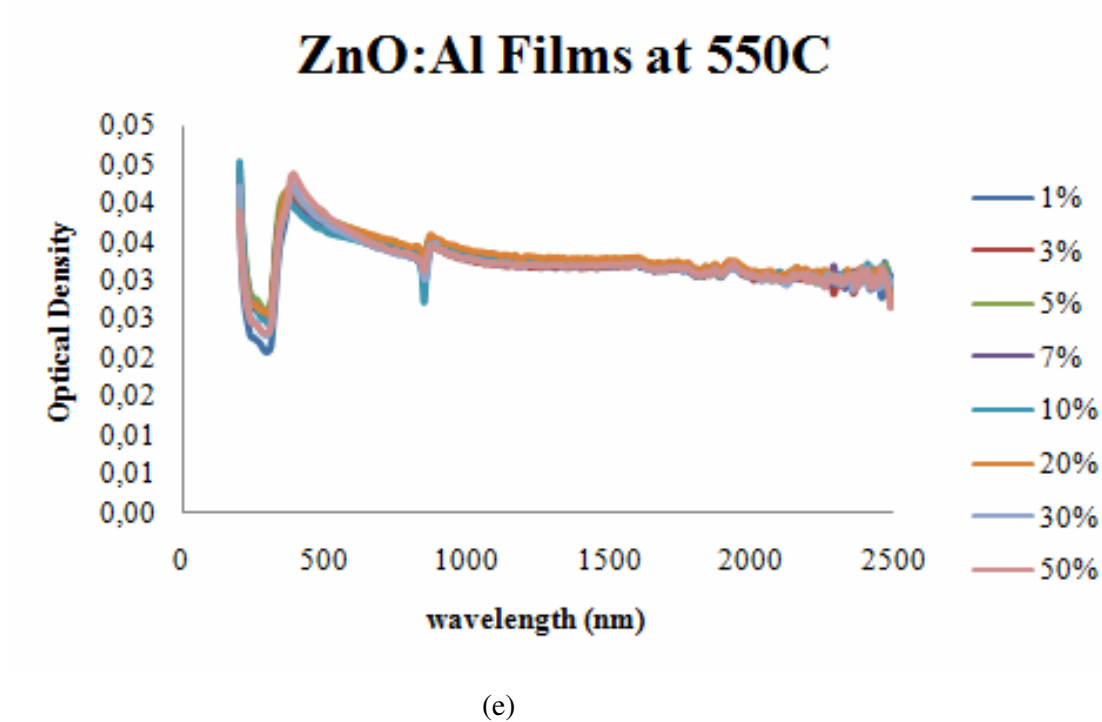

(a)

(b)
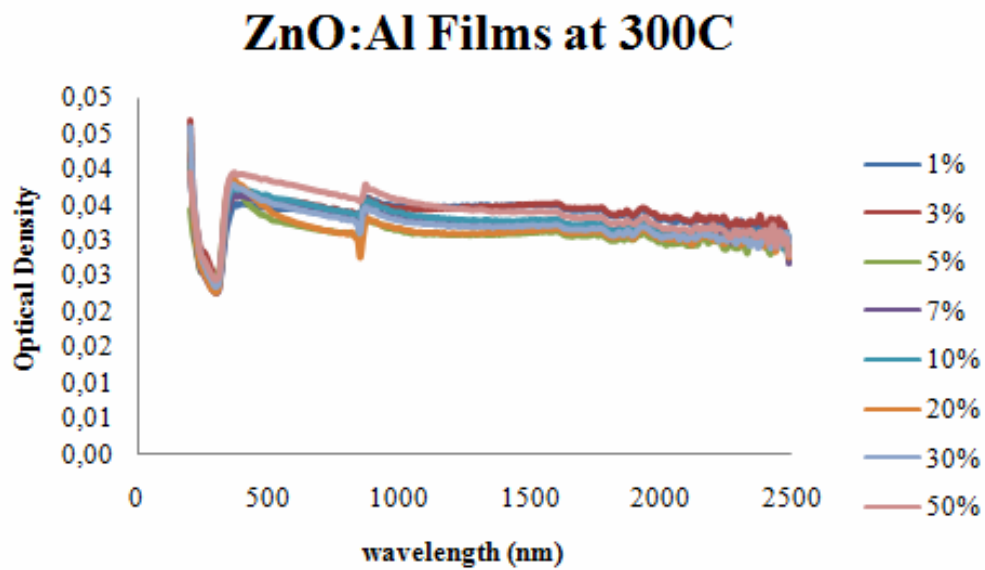
ZnO:Al Films at 400C

(c)

ZnO:Al Films at 500C

(d)

ZnO:Al Films at 550C

(e)

Figure 7.6: Effect of dopant concentration over optical densities at (a) 200°, (b) 300°C, (c) 400°C, (d) 500°C and (e) 550°C postheating temperatures

The optical band gaps of the Al doped ZnO films postheated at different temperaures, are presented in Figure 7. There are two types of optical transitions that can occur at the fundamental edge: direct and indirect. Both involve the interaction of an electromagnetic wave with an electron in the valance band, which is raised across the fundamental gap to the conduction band. However, indirect transitions also involve simultaneous interaction with lattice vibrations. Thus, the wave vector of the electron can change in the optical transition, the momentum change being taken or provided by phonons.

Transitions involving no phonons are called direct transitions and those involving phonons indirect transitions. For direct transitions $n = 1/2$ or $3/2$ depending on whether the transition is allowed or forbidden in the quantum-mechanical sense. E_0 is the optical gap and n_0 refractive index in Equation 7.2 [10-26];

$$\alpha n_0 \hbar \omega \sim (\hbar \omega - E_0)^n \qquad \textbf{(7.3)}$$

In an allowed direct transition, α is given in Equation 7.3. Where A is a constant;

$$\alpha = A(h\gamma - E_0)^{1/2}$$

Plots of $(\alpha h v)^2$ versus $h v$ and $(\alpha h v)^{1/2}$ versus $h v$ were analysed and better linearity was observed for the optical band gap as shown in Figure 7.7 . For this study, n value is determined as 1/2 for $(\alpha h v)^{1/n}$. From the plot, the band gap energy was determined by extrapolating the linear portion of the graph to $h v = 0$. It is determined that there is an allowed direct transition as $(\alpha h v)^2$ for ZnO film.

The effect of dopant concentration on allowed direct transition and optical band gap of at 200°C, 300°C, 400°C, 500°C and 550°C are shown in Figure 7.7 .
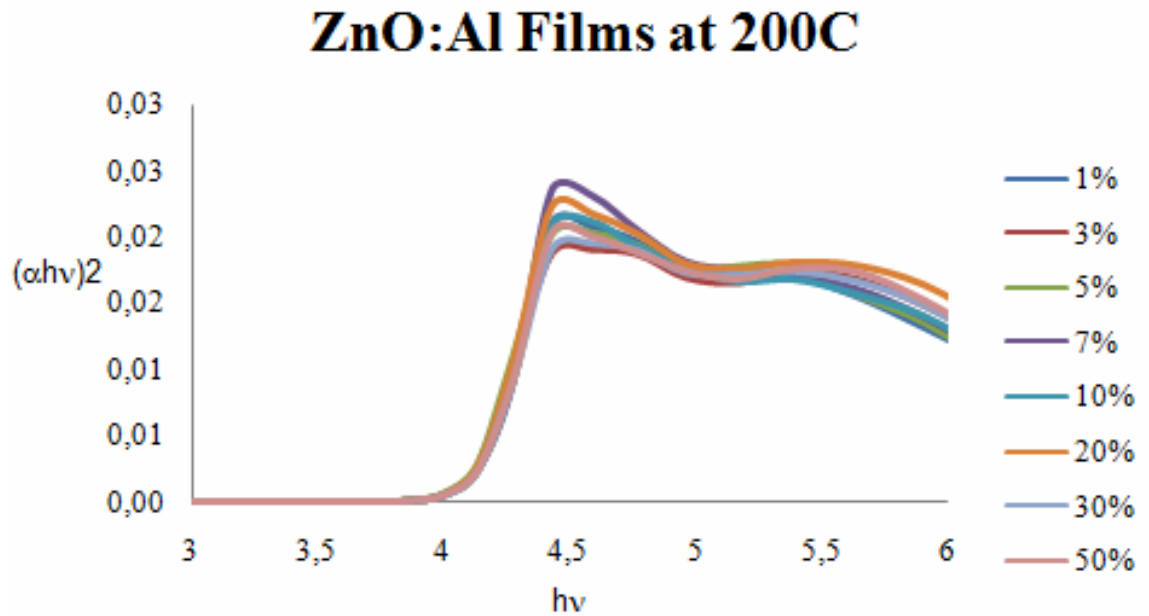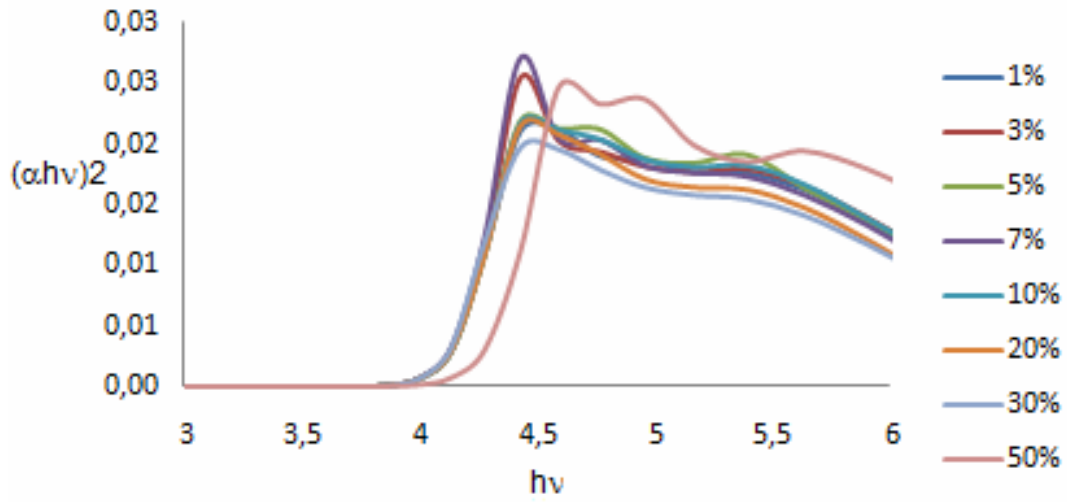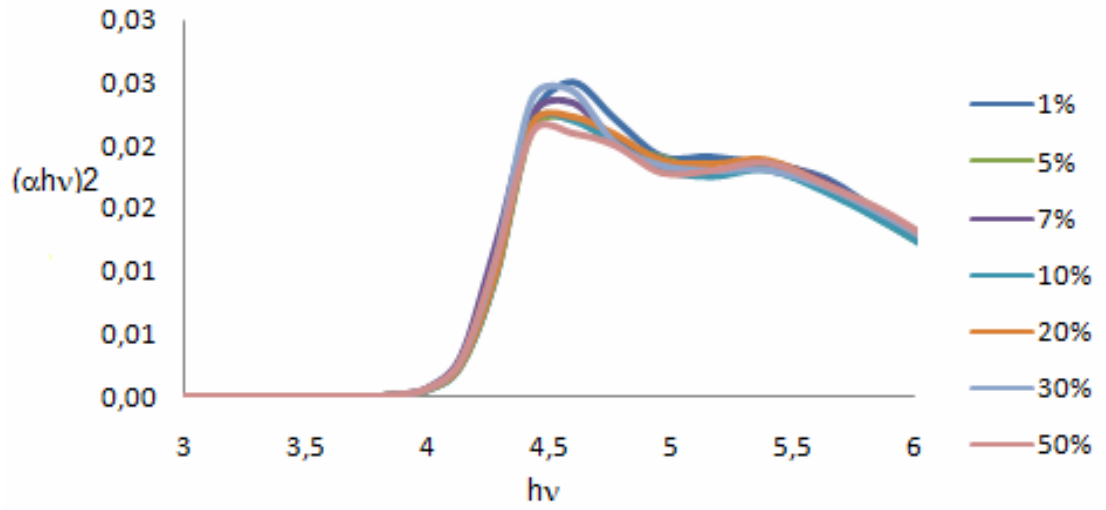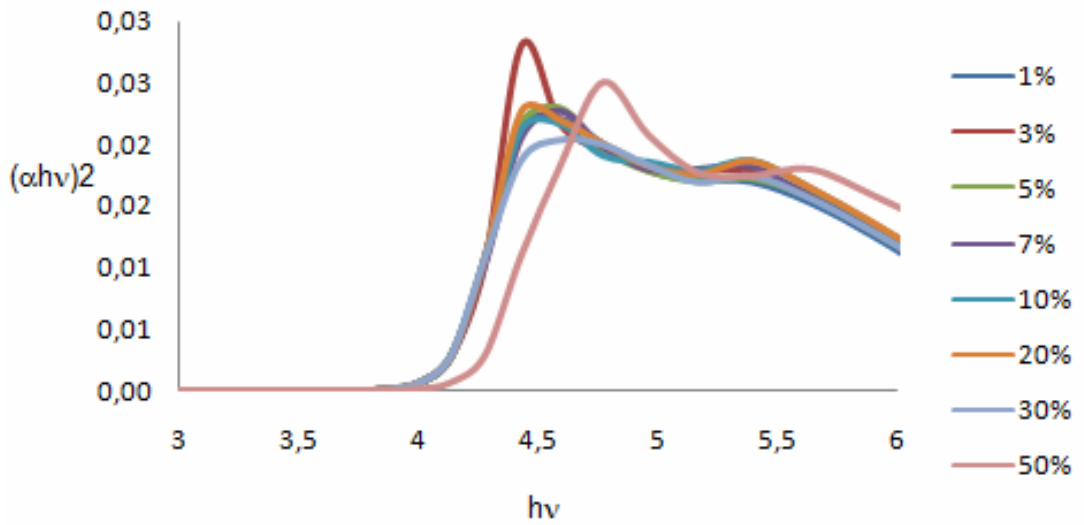
ZnO:Al Films at 200C

(a)

ZnO:Al Films at 300C

(b)

ZnO:Al Films at 400C

(c)

(d)
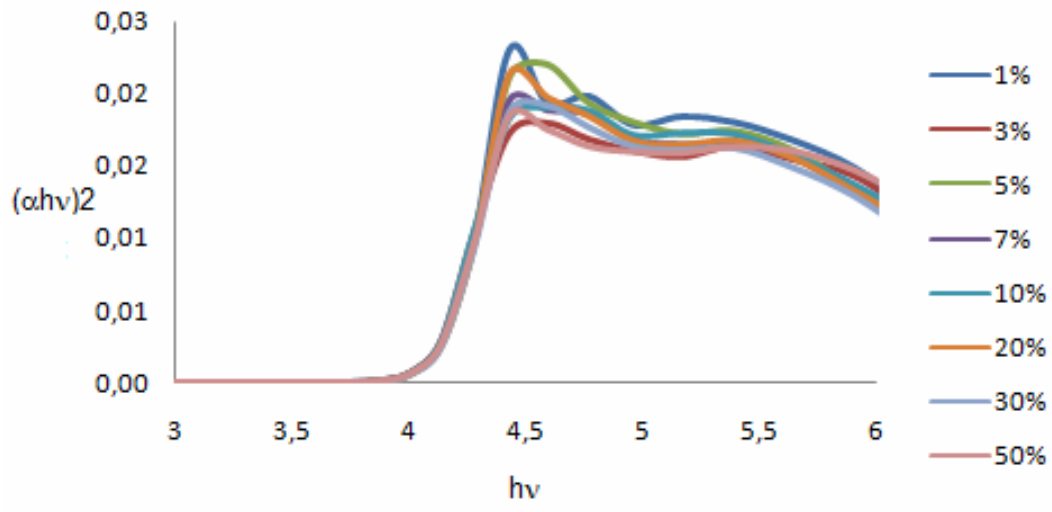
(e)

Figure 7.7: Allowed direct transition and optical band gap of AZO thin films

Transmittance (T, %) of unirradiated and irradiated ZnO films postheated at five different temperatures (in between 100°C and 500°C). The difference between the transmittance of unirradiated and irradiated ZnO films became apparent after the postheating temperature of 300 °C, which was reported as the crystalization starting temperature for ZnO films [66]. The transmittance of the irradiated ZnO film decreased in UV range with increasing the postheating temperatures to 400°C and 500°C (Figure 7.8 (d) and (e)). Thus, the transmitance of the ZnO films postheating at 400°C and 500°C shifted to visible range of electromagnetic spectrum, after irradiation.

(a)

(b)

(c)

75
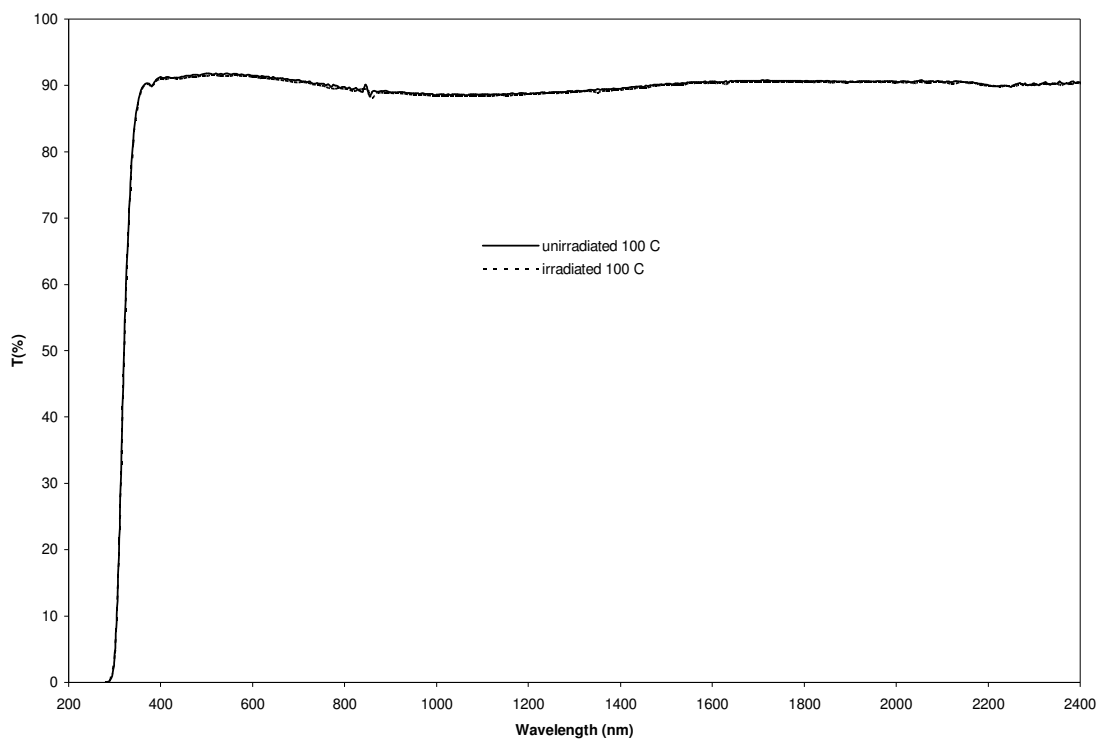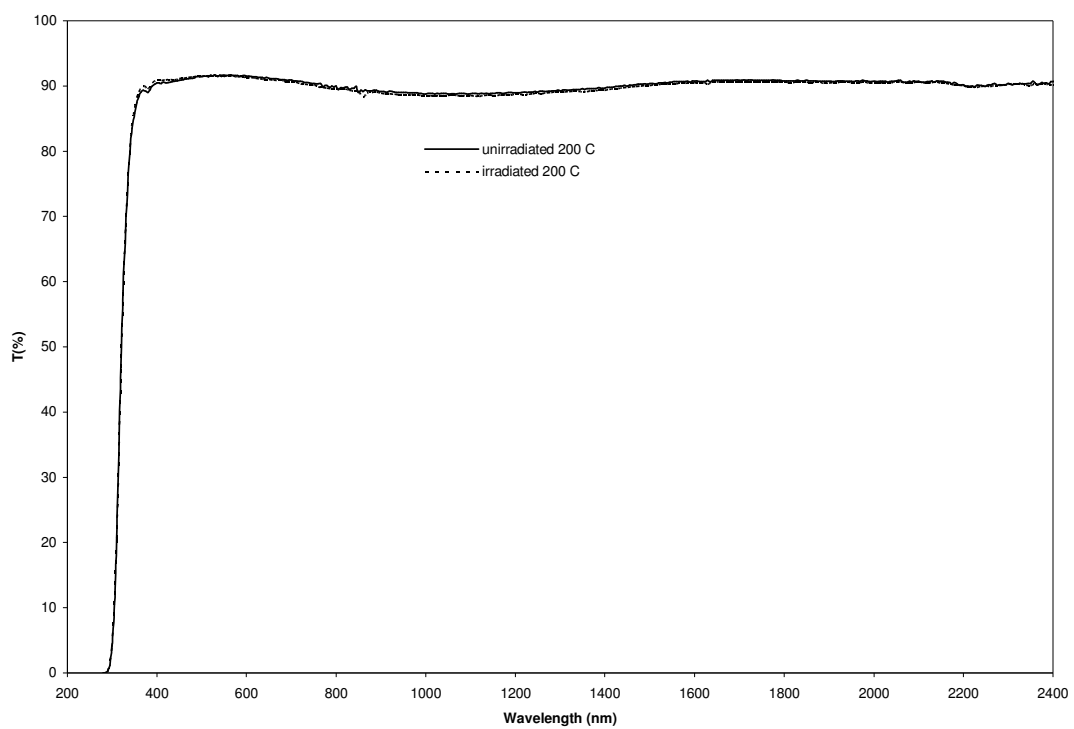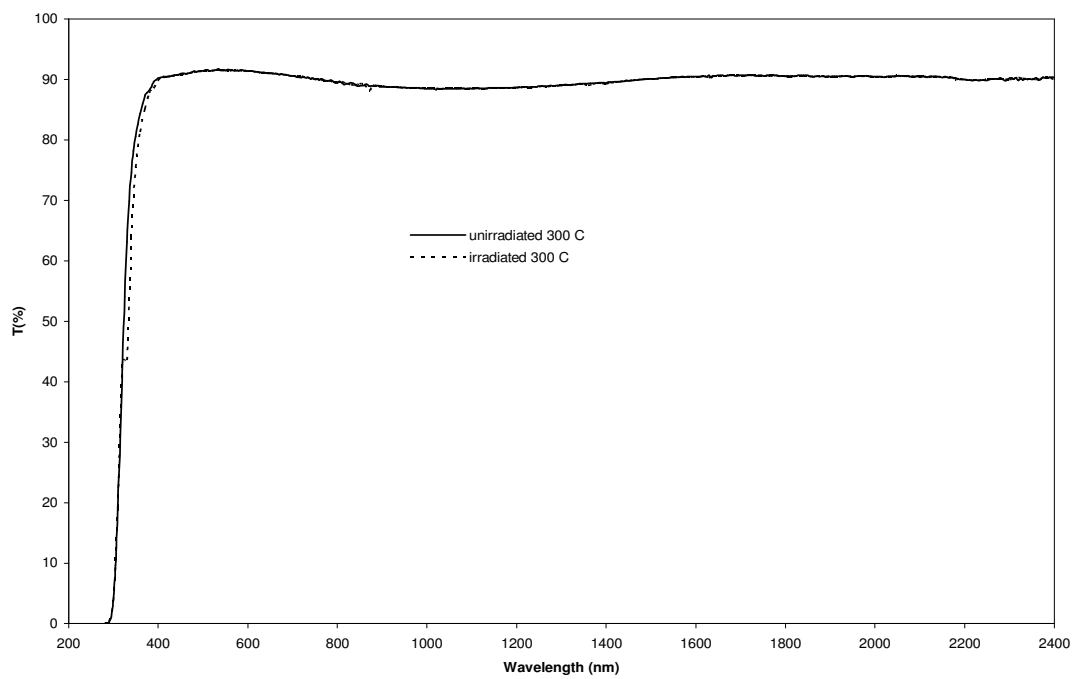
(d)

(e)

Figure 7.8: Transmittance of unirradiated and irradiated ZnO films postheated at (a) 100°C, (b) 200°C, (c) 300°C, (d) 400°C and (e)500°C

76

The effect of irradiation on ZnO films was investigated at five different postheating temperatures such as 100, 200, 300, 400, 500 °C in Figure 7.9. The transmittance of the irradiated ZnO film at 0.38 Gy changed at the visible range of the electromagnetic spectrum in Figure 7.9. When the postheated temperature of the thin f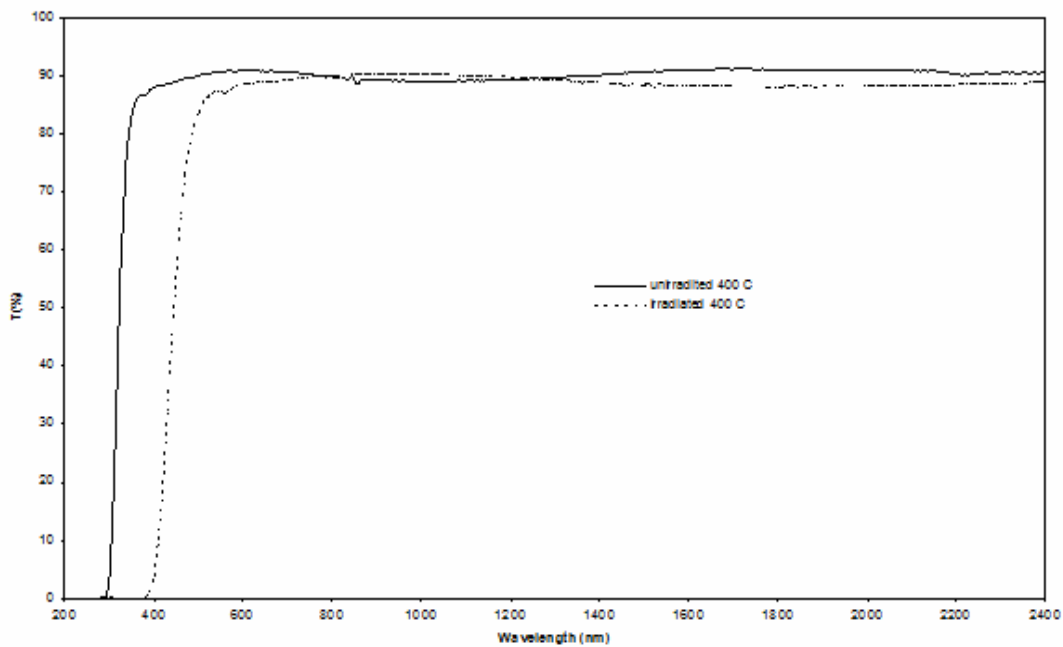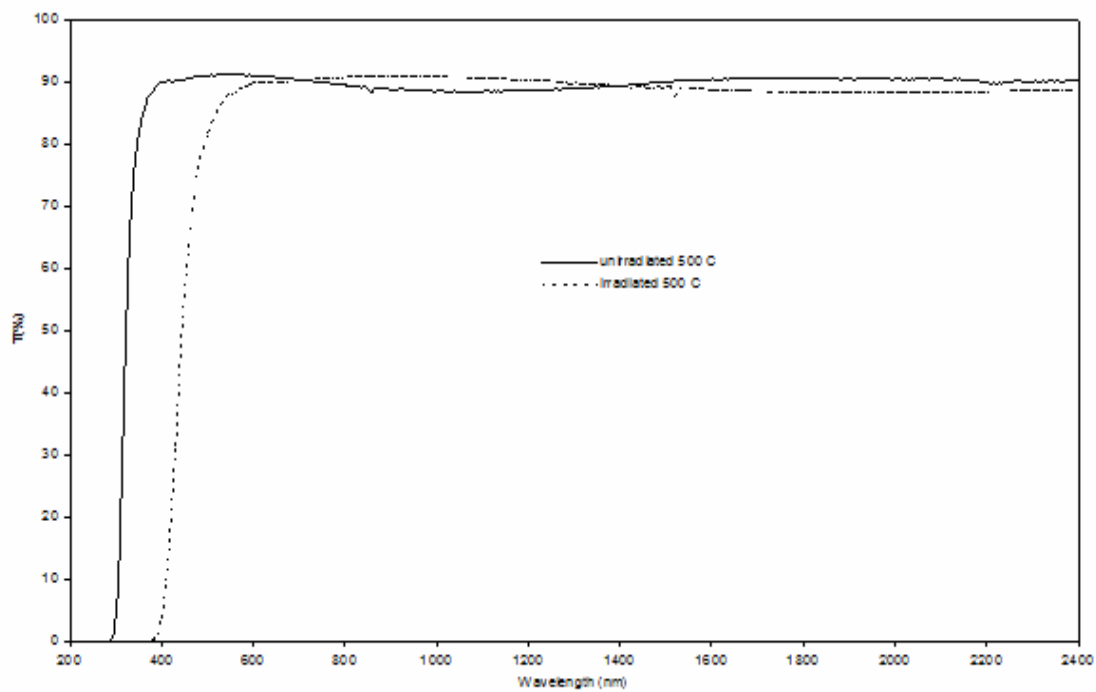ilm increased the transmittance of the induced ZnO film decreased. There is not any difference between the transmittance of unirradiated and irradiated ZnO films at the annealed temperature of 100 °C. However transmittance of the irradiated films that is annealed at 200 °C started to distinguish from unirradiated one. The transmittance of the induced film by gamma radiation is affected at the annealed temperature of 300°C in Figure 7.9 (a). When the annealing temperature of the irradiated ZnO film reached to 300°C the transmittance of irradiated film started to decrease according to the transmittance of unirradiated one. There is an interesting change at the transmittance of irradiated ZnO films that is annealed 400 °C in Figure 7.9 (b). The absorbed dose of ZnO film has reduced to the transmittance of the irradiated film at the annealed temperature of 400 °C. Besides transmittance of this film is the similar with the film at 500 °C postheating temperature.
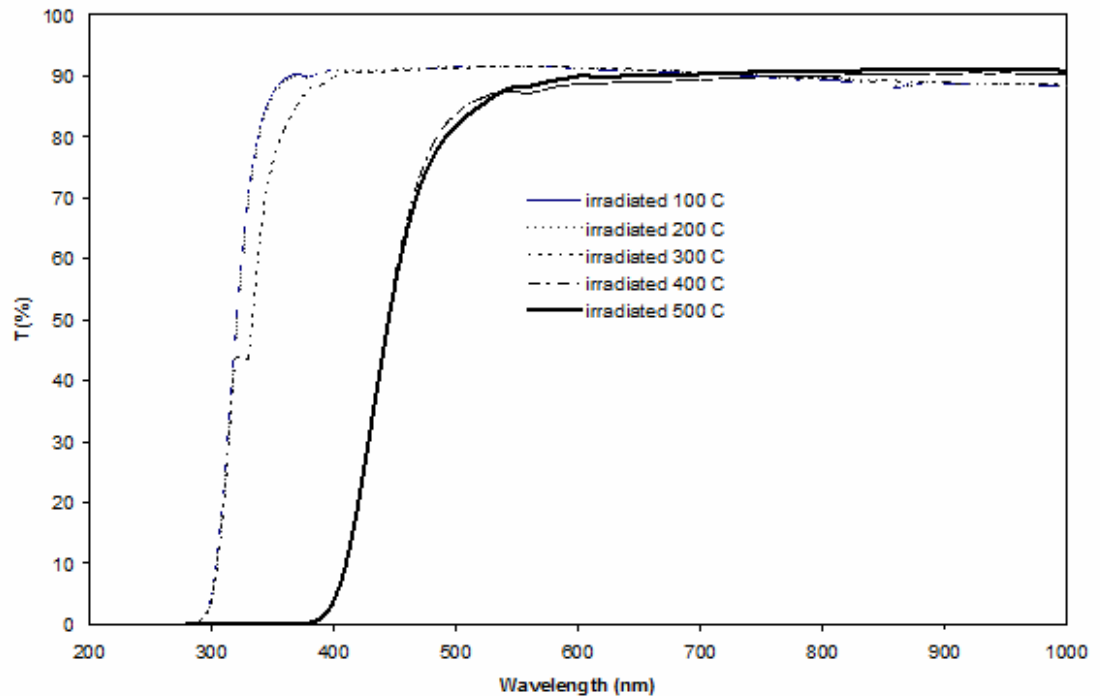
Figure 7.9: Transmittance of irradiated ZnO films at 0.38 Gy

The changes of optical density bands due to absorbed dose explain the absorption of sunlight by colour centres due to elements in the material. Optical density is evaluated depending on the wavelength is depicted in Figure 7.10. As the difference of transmittance of unirradiated and irradiated ZnO films was evident at 400 °C the optical densities of unirradiated and irradiated ZnO films were investigated at this postheating temperature. Unirradiated and irradiated ZnO films give the characteristic optical density bands at ~ 365 and ~ 370 nm respectively in Figure 7.10 below. The optical density of irradiated ZnO film has increased due to the absorbed dose of the film. Besides, the absorption band of irradiated ZnO film at 0.38 Gy shift to the visible range of electromagnetic spectrum.
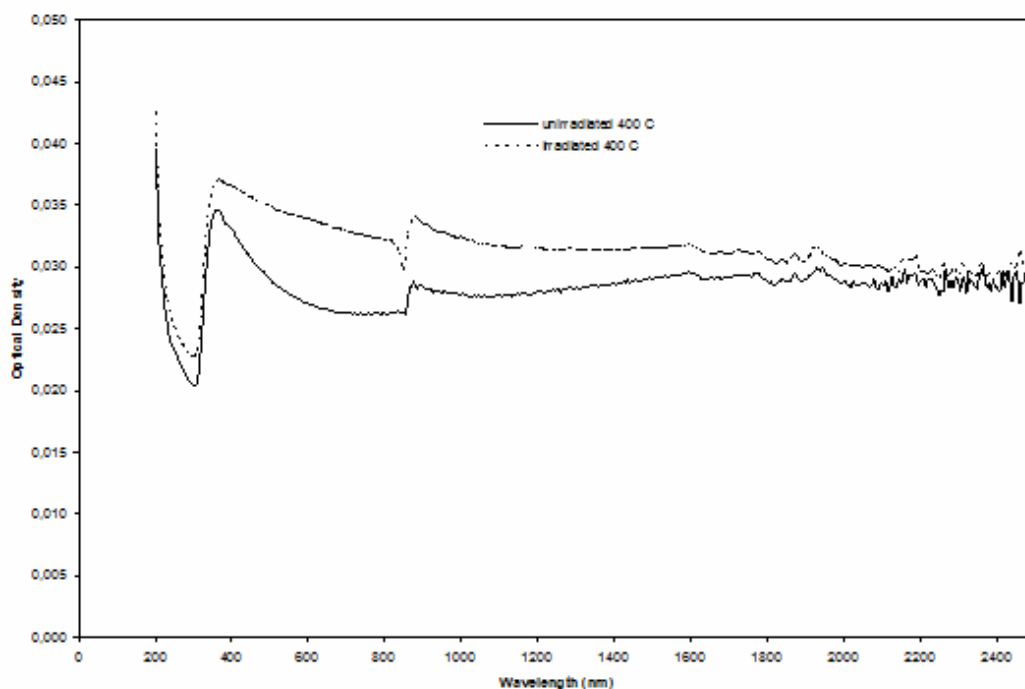
Figure 7.10: Optical densities of unirradiated and irradiated ZnO films at 400°C

When results are compared according to dopant levels it is seen that; if the dopant level of Al increased optical density increased. The dopant level of Al at 5 and 50 % mol is investigated in Figure 7.11 . Besides when the annealed temperature increased from 300 °C to 550 °C optical density of the film changed.
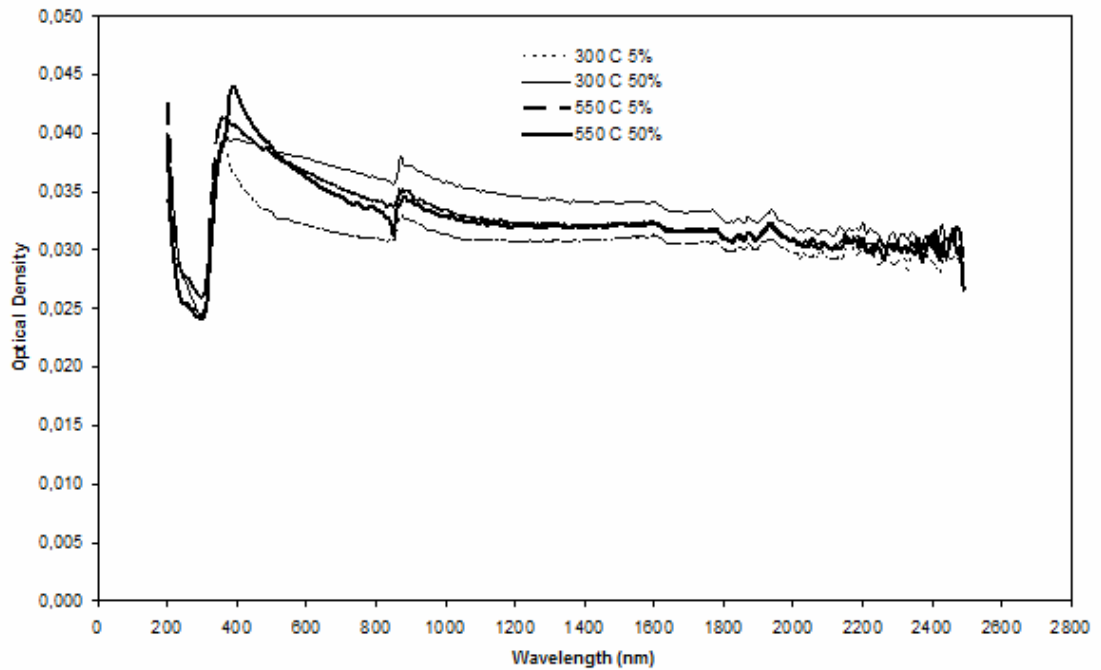
Figure 7.11 : The dopant level effect on optical density at 300°C and 550°C

The optical band gap of ZnO film that is annealed at 300 C was determined as 3.50 eV. However the optical band gap of ZnO film that is annealed at 500 °C is 3.42 eV in Figure 7.12. The decrease of the optical band gap depends on the increase of the postheating temperature of ZnO film. The changes of the postheating temperature are very important for the optical band gap. It can be thought that the decrease of optical band gap is related to the colour centres at the film.
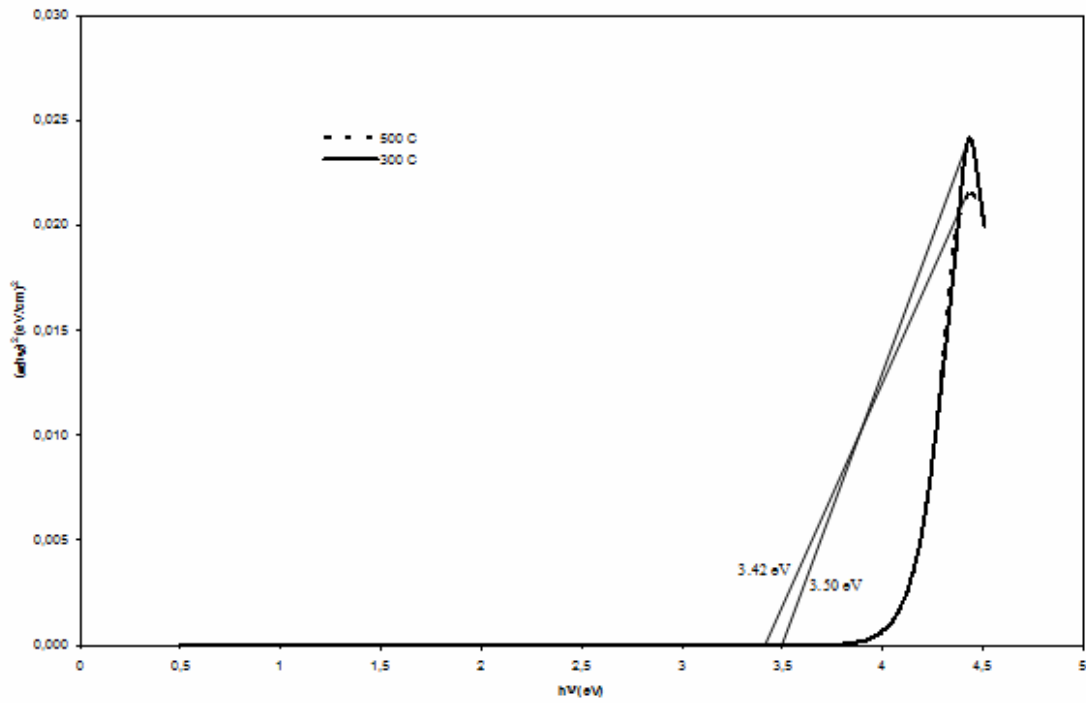
Figure 7.12: Allowed direct transition and optical band gap of ZnO film

The optical band gap of uniradiated ZnO film annealed at 500°C was determined as 3.31 eV, while it decreased to 3.11 eV upon irradiation (Figure 7.13). The decrease of optical band gap can be explained by pass of an electron in the valance band to the conduction band with a lower energy after collision of photon.
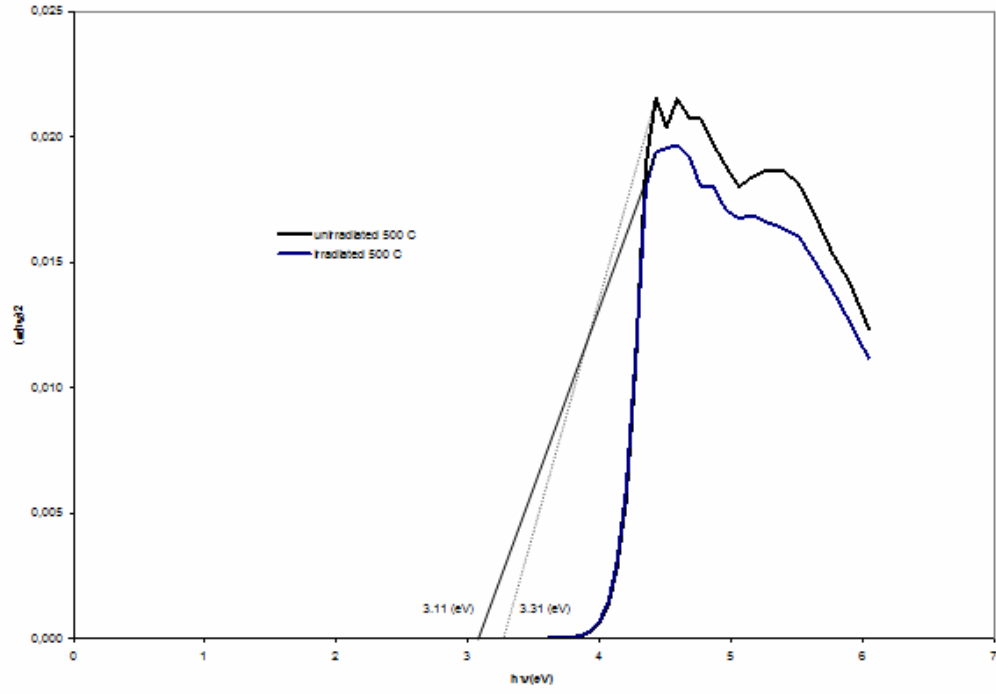
Figure 7.13: Optical band gaps of irradiated and unirradiated ZnO

7.4 Electrical Properties

The electrical properties of oxides depend critically upon the oxidation state of the metal component (stoichiometry of the oxide) and on the nature and quantity of impurities incorporated in the films, either intentiallyor inadvertently [10].

The electrical conductivity in AZO films is essentially due to the contribution from Al^{3+} ions on substitutional sites of Zn^{2+} ions and Al interstitial atoms as well as from oxygen vacancies and Zn interstitials atoms [10]. Figure 7. Shows the oxygen vacancies in ZnO structure.

(a)   (b)
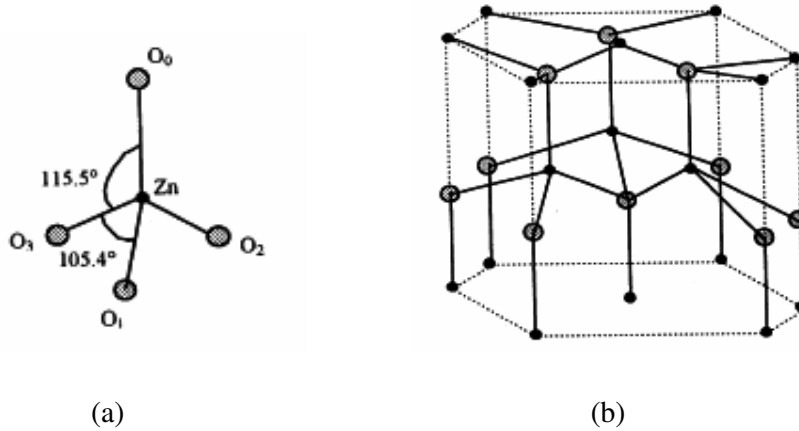
Figure 7.14: (a) Deformed coordination tetrahedron and (b) ZnO structure (black circles: zinc; grey circles: oxygen) [67].

The carrier concentration (*n*) is derived from the relation (7.5);

$$n = 1/e \cdot R_H \tag{7.5}$$

where R_H is the Hall coefficient and *e* is the absolute value of the electron charge. The carrier mobility (*μ*) is determined using the relation

$$\mu = 1/ne\rho \tag{7.6}$$

where *ρ* is resistivity [68].

By using Equation (7.5); carrier concentration is calculated as 6.616×10^{-26} m^{-3} (6.616×10^{20} cm^{-3}), which is constant for all samples.

Resistivity and carrier mobility values of samples are shown in Table 7.2 and Table 7.3, which belong to samples annealed in vacuum and in argon ambient, respectively.

Table 7.2: Resistivity and carrier mobility values of AZO films in vacuum ambient

Vacuum Ambient	Al Concentration (%)	ρ (Ω.cm) x10^{-3}	μ (cm^2/Vs)	R_H x 10^{-3}
I	0.8	1.52	0.621	-9.44
II	1.0	1.12	0.84	-9.44
III	1.2	1.05	0.898	-9.44
IV	1.6	1.00	0.94	-9.44

Table 7.3: Resistivity and carrier mobility values of AZO films in argon ambient

Argon Ambient	Al Concentration (%)	ρ (Ω.cm)	μ (cm^2/Vs) x 10^{-2}	R_H x 10^{-3}
V	0.8	0.147	6.43	-9.44
VI	1.0	0.139	6.78	-9.44
VII	1.2	0.181	5.21	-9.44
VIII	1.6	0.155	6.07	-9.44

It is known that sintering and cooling conditions have great influences on the electrical conductivity of ZnO. The AZO film resistivity is found to decrease initially with increasing annealing temperature up to 650 °C because the grain boundaries and the crystal lattice deficiencies of the film are reduced with increasing annealing temperature, resulting in an increase of the mobility of the carriers [69,16].

Due to the fact that, after observing results of 500°C and 600°C, 700°C was decided to be the final annealing temperature.

It is seen from the Table 7.2 that; resistivity values obtained from argon ambient is much more higher than those from vacuum ambient.

The increase in resistivity is believed to be due to better film crystallinity and surface morphology, which increases with an increase in substrate temperature. The decrease in values may be caused by the annealing out of point defects and interstitial impurities.

The most important parameters required for the application of ZnO:Al film as a transparent conductor are its low electrical resistivity and high optical transmittance [6]. So; due to the experiment results it can be said that Al concentration %1.2 shows the best results in argon ambient annealing.

8. CONCLUSIONS

Following conclusions can be drawn according to the results of this study:

1. Homogenous ZnO and Al doped ZnO films can be formed on a soda lime silicate and Corning 7059 glass by sol-gel process.

2. For the undoped ZnO films annealed at 400°C and 500°C irradition by a Co60 isotope results in a considerable decrease of transmittance at UV range at 0,38 Gy.

3. Unirradiated and irradiated undoped ZnO films annealed at 500°C give the characteristic optical density bands at 365 - 370 nm and aproximately at 900 nm.

4. The optical band gap of the undoped ZnO film annealed at 500°C decreased from 3.31 eV to 3.11 eV upon irradiation.

5. The dopant level of Al at 5 and 50 % mol was also investigated in the present study. When the dopant level of Al increased optical density increased. Besides, when the annealed temperature increased from 300 °C to 550 °C optical density of the film changed.

6. Transparent and high conductive Al-doped ZnO thin films are on Corning 7059 glass were prepared by sol-gel method using dip coating technique for film deposition. The resistivity of the films ranges between 1.00×10^{-3} and $0.181 \ \Omega$ cm and a very good transmittance (80-90 %) within the visible wavelength region was achieved.

7. The increase of Al content from 0.8 – 1.6 % seems to improve the electrical conductivity, but the results are not very conclusive. The atmosphere during heat treatment significantly affects the conductivity of the films. The conductivity increases by heat treating in vacuum, comparing with the results obtained by heat treating in argon ambient.

8. The lowest resistivity was obtained as 1.00×10^{-3} Ω cm, which was achieved from in the film that contained 1.6 wt.% of aluminum, prepared with a withdrawal speed of 200 mm/min, preheated at 400 °C, final annealed at 700°C in vacuum condition.

REFERENCES

[1] **Sharan, M. A.,** 2009. Efficiency enhancement of stationary solar energy based power conversion systems in Canada, *Applied Energy*, **86**, 1405-1409

[2] **Wang, M. S., Lee, K. E., Hahn, H. S., Kim, E. J., Kim, S., Chung J., S., Shin, E. W., and Park C.,** 2007. Optical and photoluminescent properties of sol-gel Al-doped ZnO thin films, *Materials Letters*, **61**, 1118-1121.

[3] **Lee, J. H., Yeo, B. W. and Park, B. O**., 2004. Effects of the annealing treatment on electrical and optical properties of ZnO transparent conduction films by ultrasonic spraying pyrolysis, *Thin Solid Films*, **457**, 333-337.

[4] **Park, W. II., Kim, J. S., Yi, G. C., Bae, M. H. And Lee H-J**., 2004. Fabrication and electrical characteristics of high-performance ZnO nanorod field effect transistors, *Applied Physics Letters*, **85**, 5052-5055

[5] **Özgür, Ü., Aliyov, Y. I., Liu, C., Teke, A., Reshchikov, M. A., Doğan, S., Avrutin, V., Cho, J. S. and Markoç, H**., 2005. A comprehensive review of ZnO materials and devices, *Applied Physics Letters*, **98**, 041301.

[6] **Yoo, J., Lee, J., Kim, S., Yoon, K., Park, I. J., Dhungel, S. K., Karunagaran, B., Mangalaraj, D. and Yi, J**., 2005. High transmittance and low resistive ZnO:Al films for thin film solar cells, *Thin Solid Films*, **480-481**, 213-217.

[7] **Tse, K. Y., Hng, H. H., Lau, S. P., Wang Y. G. and Yu, S. F.,** 2004. ZnO thin films produced by filtered cathodic vacuum arc technique, *Ceramics International*, **30**, 1669-1674.

[8] **Tay, B. K., Zhao, Z. W. and Chua, D. H. C**., 2006. Review of metal oxide films deposited by filtered cathodic vacuum arc technique, *Materials Science and Engineering R 52*, 1-48

[9] **Musat, V., Teixeria, B., Fortunato, E., Monteiro, R. C. C. and Vilarinho, P**., 2004. Al-doped ZnO thin films by sol–gel method, *Surface and Coatings Techology*, **180-181**, 659-662.

[10] **Tahar, R. B. H**., 2005. Structural and electrical properties of aluminum-doped zinc oxide films prepared by sol–gel process, *Journal of the European Ceramic Society*, **25**, 3301-3306.

[11] **Serier H., Gaudon, M. and Menetrier, M**., 2009. Al-doped ZnO powdered materials: Al solubility limit and IR absorption properties, Solid State Sciences, In Press.

[12] **Fukuoka, O., Matsunami, N., Tazawa, M., Shimura, T., Sataka, M., Sugai, H. and Okayasu, S**., 2006. Irradiation effects with 100 MeV Xe ions on optical properties of Al-doped ZnO films, *Nuclear Instruments and Methods in Physics Research Section B: Beam Interactions with Materials and Atoms*, **250**, 295-299.

[13] **Benelmadjat, H., Boudine, B., Halimi, O. and Sebais, M**., 2009. Fabrication and characterization of pure and Sn/Sb-doped ZnO thin films deposited by sol–gel method, *Optics & Laser Technology,* **41**, 630-633.

[14] **Uhlman, D. R., Suratwala, T., Davidson, K., Boulton, J. M. and Teowee, G**., 1997. Sol-gel derived coatings on glass, *Journal of Non-crystalline Solids*, **218**, 113-122.

[15] **Zurlini, P., Lorenzi, A., Alfieri, I., Gnappi, G., Montenero, A., Senin, N., Groppetti, P. and Fabbri, P.,** 2009. Titanium and Zirconium hard coatings on glass substrates prepared by the sol-gel method, *Thin Solid Films*, In Press.

[16] **Lee, K. E., Wang, M., Kim, E. J., Hahn, S. H.,** 2009. Structural, electrical and optical properties of sol–gel AZO thin films, *Current Applied Physics*, **9**, 683-687.

[17] **Tsang, W. M., Wong, F. L., Fung, M. K., Chang, J. C., Lee, C. S., Lee, S. T**., 2008, Transparent conducting aluminum-doped zinc oxide thin film prepared by sol–gel process followed by laser irradiation treatment, *Thin Solid Films,* **517**, 891-895.

[18] **Perez, R. C., Sandoval, O. J., Sandoval, S. J., Marin, J. M., Galvan, A. M., Delgado, G. T., Alvarez, A. M.,** 1999, Influence of annealing temperature on the formation and characteristics of sol-gel prepared ZnO films, *Journal of Vacuum Science and Technology A*, **17**, 1811-1816.

[19] http://www.chemat.com/html/solgel.html accessed at 22/04/09.

[20] **Silva, R. F., Zaniquella, M. E. D**., 2004, Aluminium-doped zinc oxide films prepared by an inorganic sol–gel route, *Thin Solid Films*, **449**, 86-93.

[21] **Blees, M. H., Winkelman, G. B., Balkenende, A. R., Toonder, J. M. J**., 2000. The effect of friction on scratch adhesion testing: application to a sol–gel coating on polypropylene, *Thin Solid Films*, **359**, 1-13.

[22] **GranqvistÃ, C. G.,** Transparent conductors as solar energy materials: A panoramic review, 2007, *Solar Energy Materials & Solar Cells* , **91**, 1529-1598.

[23] **Li, C., Furuta, M., Matsuda, T., Hiramatsu, T., Furuta, T., Hirao, T.,** 2009. Effects of substrate on the structural, electrical and optical properties of Al-doped ZnO films prepared by radio frequency magnetron sputtering, *Thin Solid Films,* 517, 3265-3268.

[24] **Sahal, M., Hartiti, B., Ridah, A., Mollar, M., Mari, B.,** 2008. Structural, electrical and optical properties of ZnO thin films deposited by sol–gel method, *Microelectronics Journal,* 39, 1425-1428.

[25] **Stoch, A., Jastrzebski, W., Długoń, E., Lejda, W., Trybalska, B., Stoch, G. J., Adamczyk, A.,** 2005. Sol–gel derived hydroxyapatite coatings on titanium and its alloy Ti6Al4V, *Journal of Molecular Structure,* **744-747**, 633-640.

[26] **Dunn, B., Zink, J. I**., 2007. Sol-gel chemistry and materials, *Accounts of Chemical Research*, **40(9)**, 729.

[27] **Jones, C. T**., 2000. Dip coating, *Metal Finishing*, **98(6)**, 172-174

[28] http://www.e-flex.co.kr/product/system_dc_img02.gif accessed at 21/04/09.

[29] **Lee, W., Dwivedi, R. P., Hong, C., Kim, H. W., Cho, N. Lee, C**., 2008. Enhancement of the electrical properties of Al-doped ZnO films deposited on ZnO-buffered glass substrates by using an ultrathin aluminum underlayer, *Journal of Materials Science,* **43(3)**, 1159-1161.

[30] **Du, H., Gong, J., Sun, C., Lee, S. W., Wen, L. S**., 2004. Carrier density and DC conductivity of ultrathin aluminum films, *Journal of Materials Science,* **39(8)**, 2865-2867.

[31] **Kandrina, Y. A., Babushkin, A. N**., 2008. High-pressure electrical properties of CdS studied by impedance spectroscopy, *Inorganic Materials,* 44(5), 457-459.

[32] **Wang, J., Meng, L., Qi, Y., Li, M., Shi, G., Liu, M.,** 2009. The Al-doping contents dependence of the crystal growth and energy band structure in Al:ZnO thin films, *Journal of Crystal Growth,* 311(8), 2305-2308.

[33] **Mende, L. S., MacManus-Driscoll, J. L**., 2007. ZnO – nanostructures, defects, and devices, *Materials Today*, **10(5)**, 40-48.

[34] **Ruske, F., Pflug, A., Sittinger, V., Szyszka, B., Greiner, D., Rech, B**., 2009. Optical modeling of free electron behavior in highly doped ZnO films, *Thin Solid Films*, In Press.

[35] **Kang, H. S., Kim, G. H., Lim, S. H., Chang, H. W., Kim, J. H., Lee, S. Y**., 2008. Relationship between ultraviolet emission and electron concentration of ZnO thin films, *Thin Solid Films*, **516(10)**, 3147-3151.

[36] **Batista, J., Mandelis, A., Shaughnessy, D**., 2003. Temperature dependence of carrier mobility in Si wafers measured by infrared photocarrier radiometry, *Applied Physics Letters*, **82**, 4077.

[37] **Zhang, Y., Tan, Y. W., Storner, H. L., Kim, P**., 2005. Experimental observation of the quantum Hall effect and Berry's phase in graphene, *Nature*, **438**, 201-204.

[38] **Agarwal, D. B**., 1961. Hall mobility of degenerate semiconductors, *Zeitschrift für Physik*, **163**, 207-210.

[39] **Madelung, O. , Rössler, U. and Schulz, M**., 2006. Amorphous silicon (a-Si) hall mobility and magnetoresistance, *Springer-Verlag*, **41E**, 1-2.

[40] **Hwang, C. Y., Schurman, M. J., Mayo, W. E., Lu, Y. C., Stall, R. A., Salagaj, T.,** 1997. Effects of structural defects and chemical impurities on Hall mobilities in low pressure MOCVD grown GaN, *Journal of electronic materials*, **26(3)**, 243.

[41] **Studeniken, S. A., Golego, N., Cocivera, M**., 2000. Carrier mobility and density contributions to photoconductivity transients in polycrystalline ZnO films, *Journal of Applied Physics*, **87**, 2413-2420.

[42] **Van der Pauw, L. J**., 1958. A method of measuring specific resistivity and Hall effect of discs of arbitrary shape, *Philips Research Reports*, **13**, 1-9.

[43] **Smalley, R. E**., 2005. Future global energy prosperity, the terawatt challenge, *MRS Bulletin*, **30**, 412-417.

[44] **Ratana, T., Amornpitoksuk, P., Ratana, T., Suwanboon, S.,** 2009. The wide band gap of highly oriented nanocrystalline Al doped ZnO thin films from sol–gel dip coating, *Journal of Alloys and Compounds,* **470**, 408-412.

[45] **Fernandez, S., Martínez-Steele, A., Gandía, J. J., Naranjo, F. B**., 2009. Radio frequency sputter deposition of high-quality conductive and transparent ZnO:Al films on polymer substrates for thin film solar cells applications, *Thin Solid Films,* **517**, 3152-3156.

[46] **Hemissi, M., Amardjia-Adnani, H., Plenet, J. C**., 2009. Titanium oxide thin layers deposed by dip-coating method: Their optical and structural properties, *Current Applied Physics,* **9**, 717-721.

[47] **Sabataityte, J., Oja, I., Lenzmann, F., Volobujeva, O.,Krunks, M**., 2006. Characterization of nanoporous TiO_2 films prepared by sol-gel method, *Comptes Rendus Chimie*, **9**, 708-712.

[48] NASA Space Vehicle Design Criteria (atructure). Nuclear and space radiation effects on materials, NASA SP-8053

[49] Springer Berlin Heidelberg, Modeling Solar Radiation at the Earth's Surface, modeling irradiation estimation methods from sunshine and cloud cover data, 2008, 145-173.

[50] **Peterson, J., Macdonell, M., Haroun, L., Monette, F**., 2007. Radiological and chemical fact sheets to support health risk analyses for contaminated areas, *Argonne National Health Laboratory Environmental Science Division*.

[51] **Özdemir, Ö., Çimenoğlu, H., Baydoğan, N., Sengel, H., Akmaz, F., Parlar A**.,2009. Optical and Electrical Properties of Al Doped ZnO Transparent Film Irradiated by Co-60 Radioisotope, *TMS 2009*, 138 th Annual Meeting & Exhibition, 30.

[52] **Furusawa, F., Terao, K., Nagasawa, N., Yoshii, F., Kubota, S., Dobashi, T**., 2004. Nanometer-sized gelatin particles prepared by means of gamma-ray irradiation, *Colloid & Polymer Science,* **283**, 229-233.

[53] **Igasaki, Y., Kanma, H**., 2001. Argon gas pressure dependence of the properties of transparent conducting ZnO:Al films deposited on glass substrates, *Applied Surface Science*, **169-170**, 508-511.

[54] http://www.bogamedical.com.tr/Bandelin.htm, accessed at 22/04/09.

[55] http://ksvltd.com/shop/prodimgs/prod_338.jpg accessed at 23/04/09.

[56] http://www.qsaglobal.com/Portals/QSASources/Skins/Sources/images/Capsules. jpg accessed at 23/04/09.

[57] **Baydogan, N., Zayim, E., Tugrul, A. B**., 2007. Solar parameters of induced WO$_3$-coated glass, *Nuclear Instruments and Methods in Physics Research*, **B 264**, 302-310.

[58] http://www.argus-hazco.com/images/innovx-XRF-Analyzer.jpg accessed at 23/04/09.

[59] http://www.bo.imm.cnr.it/site/files/dektak.jpg accessed at 23/04/09.

[60] **Kuo, S. Y., Chen, W. C., Lai, F. I., Cheng C. P., Kuo, H. C., Wang, S. C., Hsieh, W. F**., 2006. Effects of doping concentration and annealing temperature on properties of highly oriented Al-doped ZnO films, *Journal of Crystal Growth*, **287**, 78-84.

[61] **Nijnatten, P. A**., 2009. Optical monitoring of thin film properties using in-situ measurement of transmittance and reflectance, *Thin Solid Films,* **517**, 3087-3091.

[62] **Fujihara, S., Kishiki, Y., Kimura, T**., 2001. Crystallization behavior and origin of *c*-axis orientation in sol–gel-derived ZnO:Li thin films on glass substrates, *Applied Surface Science,* **180**, 341-350.

[63] **Yadav, R. S., Mishra, P., Pandey, A. C**., 2008. Growth mechanism and optical property of ZnO nanoparticles synthesized by sonochemical method, *Ultrasonics Sonochemistry,* **15**, 863-868.

[64] **Baydogan, N**., 2004. Evaluation of optical properties of the amorphous carbon film on fused silica, *Materials Science and Engineering*, **B107**, 70-77.

[65] **Baydogan, N., Tugrul, A. B**., 2006. Evaluation of the optical changes for a soda-lime-silicate glass exposed to radiation, *Glass Physics and Chemistry*, **32(3)**, 309-314.

[66] **Silva, R. F., Zaniquelli, M. E. D**., 2002. Morphology of nanometric size particulate aluminum-doped zinc oxide films, *Colloids and Surfaces A: Physicochemical and Engineering Aspects*, **198-200**, 551-558.

[67] **Smith, A., Rodriguez-Clemente, R.**, 1999. Morphological differences in ZnO films by the prosol technique: effect of HCl, *Thin Solid Films*, **345**, 192-196.

[68] **Gupta, R. K., Ghosh, K. Patel, R., Mishra, S. R., Kahol, P. K**., 2009. Preparation and characterization of highly conducting and transparent Al doped CdO thin films by pulsed laser deposition, *Current Applied Physics*, **9**, 673-677.

[69] **Zhen, Z., Kato, K., Komaki, T., Yoshino, M., Yukawa, H., Morinaga, M., Morita, K**., 2004. Effects of dopants and hydrogen on the electrical conductivity of ZnO, *Journal of the European Ceramic Society* , **24**, 139-146.

CURRICULUM VITA

Candidate's full name: Özge ÖZDEMİR

Place and date of birth: Eskişehir / 06.05.1982

Permanent Address: 19 Mayıs Mah. Mehmetler Sk. Altıkardeşler Apt. NO:5
D:29 Şişli / İstanbul

Universities and
Colleges attended: Anadolu University

Materials Science and Engineering

Publications:

- Karasu, B., Kaya, G., Özdemir, Ö. "Use of Borax Solid Wastes in Floor Tile Glazes" Sohn International Symposium on Advanced Processing of Metals and Materials: Principles, Technologies and Industrial Practice**,** San Diego, America, pp. 529-534, August 2006

- Kaya, G., Karasu, B., Özdemir, Ö. "Improvement on the Usability of Fast Fired Floor Tile Glass-Ceramic Glaze System", 4th International Conference on Advanced Materials and Processing, New Zeland, 2006.

- Kaya, G., Karasu, B., Özdemir, Ö., "The Development of Diopside Based Glass-Ceramic Glazes Suitable for Fast Fired Floor Tiles", VI. International Ceramic Congress, Sakarya, 473-478, 2006.

- Ö. Özdemir, H. Çimenoğlu, B. Tuğrul, G. Albayrak, N. Baydoğan, N. Altınsoy, M. Baydoğan, H.Sengel, F. Akmaz, A. Parlar, 2008, The Optical Behavior Of Zno Films Against The Radiation, 14th International Metallurgy & Materials Congress (IMMC 2008), pp. 1652-1659, TÜYAP Fair, Convention and Congress Center, October 16 - 18, İstanbul 2008.

- Ö. Özdemir, H. Çimenoğlu, N. Baydoğan, H.Sengel, F. Akmaz, A. Parlar, Optical and Electrical Properties of Al Doped ZnO Transparent Film Irradiated by Co-60 Radioisotope, TMS 2009, 138 th Annual Meeting & Exhibition, pp. 30, February 15-19, 2009, San Francisco, California

- Ö. Özdemir, H. Çimenoğlu, N. Baydoğan, H.Sengel, F. Akmaz, A. Parlar, 2008, The Optıcal Propertıes Of The Al:ZnO Thın Fılms Irradıated By Co-60 Radıoısotope, The Fifth Eurosion Conference on Nuclear Science and Its Applications, 14-17 October 2008, Ankara, pp. 170.

- M. Tekin, H. Tuğral, Ö. Özdemir, H. Çimenoğlu, E. S. Kayalı, A. B. Tuğrul, N. Baydoğan, M. Baydoğan, N. Altınsoy, G. Albayrak, H. Sengel, F. Akmaz, A. Parlar, Investigation of Heat Treatment and Al Doping On Irradiated Nanosize Hexagonal ZnO, 5th International Advanced Technologies Symposium (IATS 09), May 13-15, 2009, Karabuk, Turkey.(Sunuma kabul edilmiştir.)